DISCHARGE INITIATION EXPERIMENTS IN THE TOKAPOLE II TOKAMAK

by

DAVID ADNA SHEPARD

A thesis submitted in partial fulfillment of the

requirements for the degree of

Doctor of Philosophy

(Physics)

at the

UNIVERSITY OF WISCONSIN-MADISON

1984



DISCHARGE INITIATION EXPERIMENTS

IN THE TOKAPOLE II TOKAMAK

David Adna Shepard

(Under the supervision of Associate Professor Stewart C. Prager)

Experiments in the Tokapole II tokamak demonstrate the benefits of high density ($n_e/n_o > 0.01$) preionization by reducing four quantities at startup: necessary toroidal loop voltage ($V_1$) (50%), volt-second consumption (40-50%), impurity radiation (25-50%), and runaway electron production (~ 80-100%). A zero-dimensional code models the loop voltage reduction dependence on preionization density and predicts a similar result for reactor scale devices. The code shows low initial resistivity and a high resistivity time derivative contribute to loop voltage reduction.

Microwaves at the electron cyclotron resonance (ECR) frequency and plasma gun injection produce high density preionization, which reduces the initial $V_1$, volt-second consumption, and runaways. The ECR preionization also reduces impurity radiation by shortening the time from voltage

application to current channel formation. This, evidently, reduces the total plasma-wall interaction at startup.

The power balance of the ECR plasma in a toroidal-field-only case was studied. Langmuir probes and impurity doping were used. The vertical electric field ($E_v$) and current ($I_v$), which result from curvature drift, were measured ($E_v \sim 10$ V/cm and $I_v \sim 50$ Amps) and exceeded expected values for the bulk electron temperature (~10 eV). Presumably, the electron distribution function is non-Maxwellian, and the $E_v$ and $I_v$ are the result of a population of warm electrons. This is supported by impurity doping, which increases the radiated power while decreasing the warm electron signatures. Apparently, the major power losses are curvature drift and radiation. This implies favorable scaling, in which the required ECR power is linear with scale length (like radius) and not cubic (like volume).

A series of experiments with external windings to simulate field errors perpendicular to the toroidal field was done. The results imply that an error field of 0.1% of the toroidal field is deleterious to ECR plasma density. Such a field error was evidently not present during standard toroidal-field-only operation. A vertical magnetic field was capable of shortening the delay to breakdown, but could not produce the initial loop voltage reduction observed with ECR preionization.



ACKNOWLEDGMENTS

I would like to thank my advisor, Professor Stewart Prager, for his guidance throughout this research and the writing of this thesis. I would also like to thank Professors J.C. Sprott and R.N. Dexter for many helpful suggestions and discussions. In particular I thank Professor Sprott for suggesting this research topic.

The work presented in this thesis could not have been done without the assistance of my fellow graduate students and the support staff directed by T. Lovell with B. Vallem and A. Gordon. In particular, I thank A. W. Leonard who constructed the plasma gun used during a portion of this research. Dr.s R.J. Groebner, A.P. Biddle, D.J. Holly, H.R. Garner, N.S. Brickhouse, T.H. Osborne, D.W. Witherspoon, M. Zarnstroff, and Ms. T. Rempel are thanked for many hours of helpful conversation from the building of Tokapole to the present.

I wish to express my gratitude and appreciation to my parents for their love and patience throughout my student career.

I also thank my wife, Cherie, for her love and encouragement through the good and bad times. And I thank my daughters, Julie and Paula, who were often jealous of the laboratory, but who sometimes demonstrated understanding beyond their years.

Financial support for my research was provided by the U.S. Department of Energy.

TABLE OF CONTENTS

# CHAPTER I

## Introduction

### I. Motivation and Background

Discharge initiation in tokamaks is not as well understood as the steady state equilibrium. The study of gaseous electronics requires extension to toroidal systems with magnetic fields. Linear discharges have been thoroughly studied. For a typical discharge experiment, electrodes form the plasma and drive the discharge current. Usually, there is no magnetic field, and toroidicity is avoided. At startup in a tokamak, plasma formation takes place in the presence of a toroidal magnetic field, without electrodes. This is a transient and rapidly changing phase of tokamak discharges which is not well understood and is difficult to control.

In addition, tokamak studies are driven by the need for a fusion reactor. At present, toroidal systems appear to be the most easily advanced to reactor status. In particular, the tokamak concept may hold the most promise for the first-generation, deuterium-tritium-fueled reactor. The startup

of a tokamak is crucial to the feasibility of an economic reactor. The short pulse ( < 24 hrs.) devices require a startup which causes minimal damage and does not lower the efficiency. The proposed, long pulse (> 24 hrs.) devices should not be encumbered with an expensive, over-engineered, startup procedure.

The archetypical tokamak is a pulsed, toroidal, plasma confinement device of circular cross section. A toroidal loop voltage, $V_l$, breaks down the fill gas. The resultant plasma current, $I_p$, is inductively driven along the dominant, toroidal, magnetic field, $B_t$. This current produces a poloidal magnetic field, $B_p$, which pitches the total field lines into helices. The pitched field lines provide confinement against several loss mechanisms.

Some tokamaks, to which we will refer, are listed in Table 1.1. The relevant device parameters are the major radius, R, the minor radius, a, and the toroidal field, $B_t$. Plasma parameters of prime concern include $I_p$, electron density, $n_e$, and electron temperature, $T_e$. Typically, these three quantities are measured with an external rogowski coil, a microwave interferometer, and Thompson scattering, respectively.

Excellent reviews[1] explain the physics of tokamaks. The reviews also demonstrate the rise in complexity of the tokamak from its inception to a reactor candidate.



TABLE 1.1

A Representative Group of Tokamaks

| Tokamak[2] | a (cm) | R (cm) | $B_t$ (kG) | $I_p$ (kA) | $n_e$ ($cm^{-3}$) ( x $10^{13}$) | $T_e$ (eV) |
|---|---|---|---|---|---|---|
| ST | 13 | 109 | 40 | 70 | 1.5 | 2500 |
| PLT | 45 | 130 | 32 | 550 | 8 | 4000 |
| ISX-B | 27 | 93 | 12 | 100 | 6 | 1100 |
| JFT-2[3] | 25 | 90 | 10 | 70 | 1.5 | ~600 |
| Pretext[4] | 15 | 53 | <10 | 60 | 3 | 200 |
| Tokapole II[5] | 6-10 | 50 | <8 | 10-40 | 0.2-1.0 | ~100 |

Standard tokamak startup is divided into three parts: breakdown, plasma formation, and current rise [6]. This is shown schematically in Figure 1-1. $V_1$ is applied to a nearly neutral fill gas at the beginning of the breakdown phase. The departure from neutrality is a few seed electrons ($n_e/n_o \ll 1.0\%$), due to cosmic rays or a preionization source. Most devices need an electron source to assist breakdown.

Breakdown in tokamaks occurs when 1.0 to 10% of the gas is ionized for $T_e \sim 5eV$, and an electron-ion collision is as likely as an electron-neutral collision. Before breakdown is achieved, electron-neutral collisions dominate. This early phase of plasma development is characteristic of unassisted and low density ($n_e/n_o < 1.0\%$) preionization experiments. The term "high density preionization" will imply the achievement of $n_e/n_o > 1.0\%$, before $V_1$ is applied. The discussion of preionization techniques in Chapter 4 is divided into low and high density regimes.

The current profile is hollow during plasma formation, as a result of the skin effect of the plasma. The current is too low to form a tokamak equilibrium, and the energy confinement time is short. Thus, the plasma temperature is held roughly constant, below 100 eV.

Tokamak equilibrium is achieved during the current rise phase. Ionization of the gas within the hollow profile is nearly



Figure 1-1. Schematic representation of the three phases of startup: 1. Breakdown, 2. Plasma formation, and 3. Current rise.

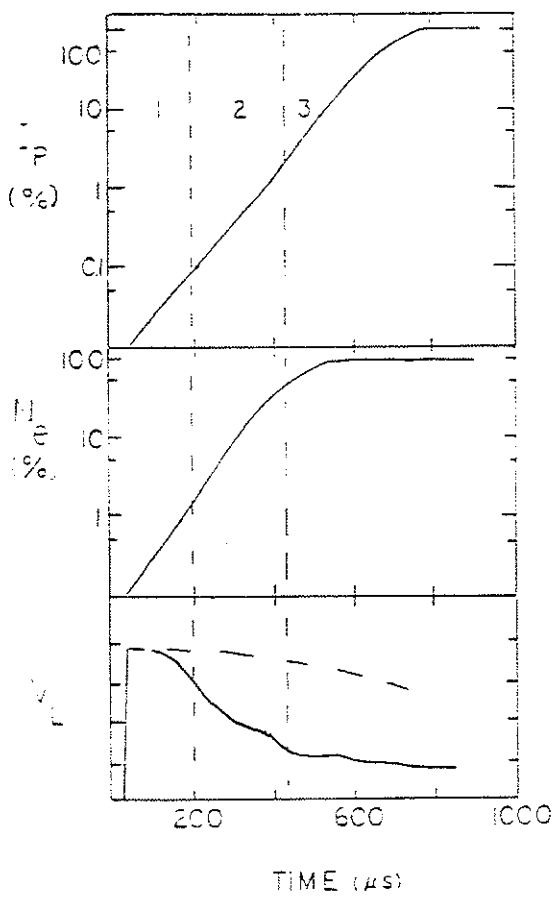




complete. The hollow current profile fills in, and energy confinement improves.

Discharge initiation topics related to gaseous electronics in toroidal magnetic fields include drifts, stray field losses, impurity radiation, and runaway electron production. These topics need to be well understood, so they may be suppressed or controlled. The effect of high density preionization on these quantities needs explanation and experimental verification. Particle drifts in a toroidal field cause severe losses before the current rise phase. Toroidal field errors create another loss channel[4,7] as particles stream parallel to B into the limiter or walls. Low-Z impurities, such as oxygen, radiate and suppress the plasma temperature, until they are "burned through".[8] This occurs when the low-Z impurities are mostly stripped of their electrons and cease to be a major loss channel. Burn-through occurs during current rise and allows temperatures to exceed 100 eV. An artifact of the early, low temperatures is a high resistivity which enhances runaway electron formation. The voltage must be held high to provide ohmic heating during breakdown and current formation, so the tail of the electron distribution function decreases in collisionality and runs away. Besides the health hazard, these runaways can cause significant material damage and impurity reflux.

The mechanisms and parameters of startup need to be understood if a tokamak reactor is to have economic feasibility. The breakdown $V_1$ scales as the major radius of a tokamak, and reactors may need hundreds of volts for startup, without high density preionization. This implies torus insulation problems, large primary voltages, and runaway electron generation. Also, the consumption of transformer volt-seconds during the non-power-producing, high-voltage startup, is a loss of efficiency.

The pulsed nature of tokamaks is unattractive to power and design engineers and material scientists. A device with the fewest possible startups under the above conditions is needed. A search for a steady state tokamak has led to non-transformer, current drive schemes. These concepts are at present too inefficient for a reactor.[9,10] Thus, an alternative approach has been suggested. A transformer-driven tokamak would be run until saturation. Non-transformer current drive would be applied while the transformer is driven to reverse saturation. This would maintain the plasma current, until the next pulse.

The eventual solution may involve a device with nearly a twenty-four-hour pulse. Such a tokamak would be part of a network which could sustain a regular but brief shutdown. This cycle could ease restrictions on ash removal and daily inspection techniques.



In summary, short-pulse (< 24 hrs.) tokamaks suffer from startup problems listed above. Long-pulse and quasi-steady-state tokamaks have fewer startups and should avoid expensive, complex startup equipment of no use during the equilibrium phase of the discharge.

In tandem with the search for long pulse devices, a different approach is desired. This approach would minimize or eliminate the objections to the startup procedure. To minimize the deleterious effects, the physics of standard startup and possible alternatives must be investigated. Also, the implications for the engineering of such devices must be clarified.

The remedy for most of the above problems proposed by this thesis is high density preionization of the startup gas. The preionization breaks down the gas before the loop voltage is applied. To understand the impact of this, the standard breakdown must be understood. Tokamak breakdown may be discussed in the framework of gaseous electronics. However, the data from gaseous electronics must be considered carefully.

Generally, unmagnetized discharges between flat plate electrodes have been studied at pressures of 0.1 to 10 torr.[11,12] Typically, kilovolts have been applied to plates separated by a few millimeters. Losses are typically governed by diffusion to the walls of the tube. An example would be a sample of gas

between two electrodes separated by a few centimeters. An increasing, from zero, voltage is applied, diffusion losses are ignored, and an ionization source is present to provide primary electrons. The sequence of events is shown schematically in Figure 1-2. At low voltages, the electrons provided by the ionization source are collected and saturation current is drawn. As the voltage increases, the primary electrons gain enough energy to ionize the sample gas. The collected current increases as the newly produced electrons produce more ionizations. This is termed the the Townsend avalanche and combined with the saturation current phase represents the Townsend discharge regime. If the ionization source is removed the discharge is terminated in this regime. At the breakdown voltage, the collected current may increase many orders of magnitude and the discharge becomes self sustaining. This occurs, if the ions produced by one primary electron release at least one secondary electron by impact at the cathode. These impact-released electrons will sustain the discharge if the ionization source is removed. The production of one secondary electron per primary electron is the Townsend criterion for breakdown.

There are major differences in the parameters of linear discharge tubes and tokamaks. Tokamaks utilize one turn voltages between 10 and 100 volts. The path length of an electron is limited by drifts and field errors, and a given electron may make



Figure 1-2. The current-voltage characteristic of a glow discharge experiment, with 1 torr of pressure.

A-B Saturation current plateau

B-C Townsend Avalanche regime

C-D Sub-normal Glow

D-E Normal Glow operation

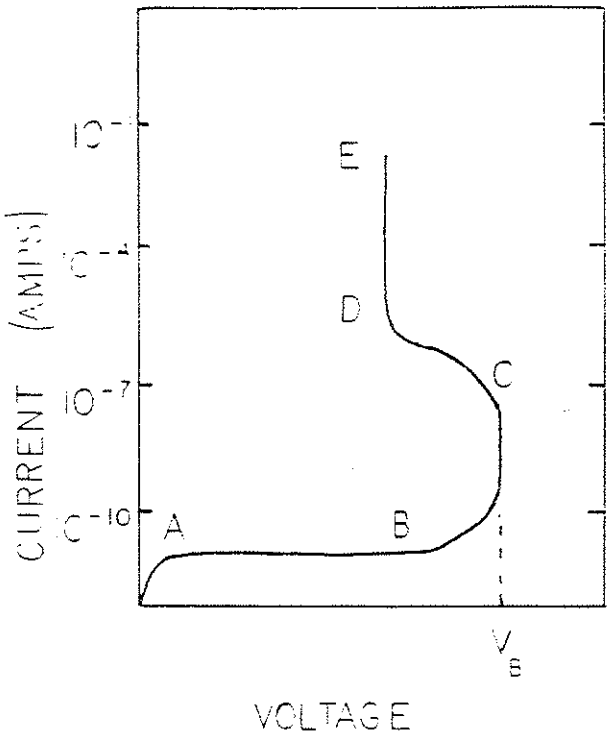




many passes through the volume of gas before being lost to a limiter. Typical fill pressures are on the order of $10^{-4}$ torr. Despite the disparity of parameters, breakdown in tokamaks is analogous to breakdown in discharge tubes. The loss mechanisms are different, but a Townsend discharge regime must develop before breakdown can occur. The phenomenology of discharge tubes has been adapted to breakdown in toroidal systems by several authors[2,13].

The linear, Extrap, Z-pinch experiment[14] provides an illustration of a system with distances nearer fusion scale lengths, a magnetic field, and voltages on the order of gaseous electronics. A voltage of > 1.0 kV is applied between electrodes 0.2 m apart. No axial magnetic field is applied, but an octupole magnetic field limits the breakdown to a narrow channel along the null and introduces a loss term which modifies the Townsend criterion. Apart from the loss term, the Townsend criterion describes the experiment. A similar loss term may affect the plasma gun preionization experiment, in Chapter Four, and will be discussed there.

The primary source of preionization plasma for this thesis is electron cyclotron resonance (ECR) frequency microwave power. Since tokamaks require auxiliary heating, there has been development of high power microwave sources which make such heating and preionization at the relevant magnetic fields (50 T)

possible. Various incarnations of the gyrotron can provide hundreds of kilowatts for preionization experiments. This raises the issue of the minimum power needed for high density preionization. To determine this, the power balance of a preionization plasma needs to be examined in the framework of a toroidal magnetic field, and gaseous dynamics.

### 1B. Outline of the Results of This Research

This thesis will describe a wide range of startup experiments done on the Tokapole II tokamak. The primary goal of this research is the understanding and lowering of the following quantities during startup: $V_1$, volt-second consumption, runaway electron production, and impurity influx. A zero-dimensional code is used to model the effects of a preionization plasma on $V_1$.

The primary tool to achieve these goals is ECR preionization at microwave frequencies. In addition, Ion Cyclotron Resonance (ICR) frequency power and gun plasma injection are tried as preionization sources.

Studies of the power balance of the ECR preionization plasma are done to reveal and possibly reduce the losses, in order to minimize the ECR power required. In addition, if the losses are



reduced, higher preionization plasma temperatures ($T_e$ > 100 eV) might burn through low-Z impurities before $V_1$ is applied. Field correction coils, electrostatic biasing of conductors in the plasma, and spectroscopic observations of impurity-doped plasmas are used.

The effects of axisymmetric vertical magnetic fields ($B_v$) are examined to achieve better particle and energy confinement. A $B_v$ field error coil and a quadrupole $B_v$ for plasma positioning are studied. The ECR plasma density prior to the application of $V_1$ and the delay to breakdown during $V_1$ application without preionization are of particular interest.

A description of Tokapole II and the available diagnostics is presented in Chapter 2. Modifications to the device during these experiments are also discussed.

Chapter 3 discusses Tokapole experiments with an ECR plasma, in a purely toroidal field, including results which imply a warm electron component dominates the power balance (50 eV < $T_e$ < 1 keV). The theoretical concerns of toroidal drifts on the plasma and microwave power accessibility to the resonance zone and coupling are briefly discussed. Some theoretical predictions, for ECR preionization, by Peng et al.[15] are reviewed. Relevant experiments in the literature are summarized for historical perspective.

Chapter 4 discusses the achievement in the Tokapole of lower startup $V_1$, volt-second consumption, runaway electron production, and impurity radiation, in light of a zero-dimensional model. Similar research elsewhere is briefly reviewed and critiqued with reference to Tokapole results.

Conclusions and suggestions for future work are presented in Chapter 5.

In this thesis, references will by made to PLP reports. These internal reports, of the University of Wisconsin Plasma Physics Group, are available on request from:

Plasma Physics Department
University of Wisconsin
1150 University Ave.
Madison, WI 53706



## References for Chapter 1

[1]L.A. Artsimovich, Nuclear Fusion, 2, 215, (1972). H.P. Furth, Nuclear Fusion, 15, 487, (1975). J. Sheffield, Proceedings of the IEEE, 69, 885, (1981).

[2]J.M. Rawls, et al., "Status of Tokamak Research,"DOE/ER-0034, U.S. Dep. Energy, Washington, DC, (1979). unless otherwise specified.

[3]R.J. La Haye, et al., Nuclear Fusion, 21, 1425, (1981)

[4]J.F. Benesch, University of Texas Ph. D. Thesis (1981).

[5]A.P. Biddle, R.N. Dexter, R.J. Groebner, D.J. Holly, B. Lipschultz, M.W. Phillips, S.C. Prager, J.C. Sprott, Nuclear Fusion, 19, 1509 (1979).

[6]R. Papoular, Nuclear Fusion, 16, 37. (1976).

[7]T. Somentani, N. Fujisawa, Plasma Physics, 20, 1101, (1978).

[8]R.J. Hawryluk and J.A. Schmidt, Nuclear Fusion,16, 775 (1976).

[9]D.F.H. Start, Nuclear Fusion, 23, 1411, (1983).

[10]J.G. Cordey, Plasma Phys. and Controlled Fusion, 26, 1A, 123, (1984).

[11]A.M. Howatson, An Introduction to Gas Discharges, Pergamon Press Ltd., (1965).

[12]A. von Engel, Electric Plasmas: Their Nature and Uses, International Publications Service Taylor and Francis Inc., (1983).

[13]D.J. Rose, M. Clark, Plasmas and Controlled Fusion, The M.I.T. Press and John Wiley and Sons, Inc., (1961).

[14]J.R. Drake, Plasma Phys. and Controlled Fusion, 26, 387, (1984).

[15]Y-K. M. Peng, B.K. Borowski, and T. Kammash, Nuclear Fusion, 18, 1489, (1978).



# CHAPTER 2

## Experimental Apparatus

### 2A. Tokapole II

The experiments reported in this thesis were carried out with the Tokapole II tokamak, shown in Figure 2-1.[1] Tokapole II has a toroidal, aluminum vacuum chamber of major radius 50 cm and a 44 cm by 44 cm square cross section, as shown in Figure 2-2. The walls are 3 cm thick to limit field soak in during the 15 ms pulse. Insulated gaps allow the magnetic fields to enter the machine.

Four internal conductors are inductively driven by the iron core transformer with total available flux of 0.15 webers. A 7.2 mF, 5 kV (90 kJ) capacitor bank with a 40:1 turns ratio on the transformer produces the sinusoidal gap voltage of half-period 5.6 ms. An active crowbar is available and has a 450 V, 0.96 F (97 kJ) capacitor bank. The internal conductors (divertors) serve to shape the tokamak cross section and to divert the tokamak edge flux. The divertors have a diameter of 5 cm and are made of a chromium-copper alloy. They are supported by rods made of a beryllium-copper alloy. Each divertor has a magnetic null and x-point region associated with it. There are three plasma regions formed by this configuration. The diverted flux is

Figure 2-1. The Tokapole II tokamak with a graduate student for scale.



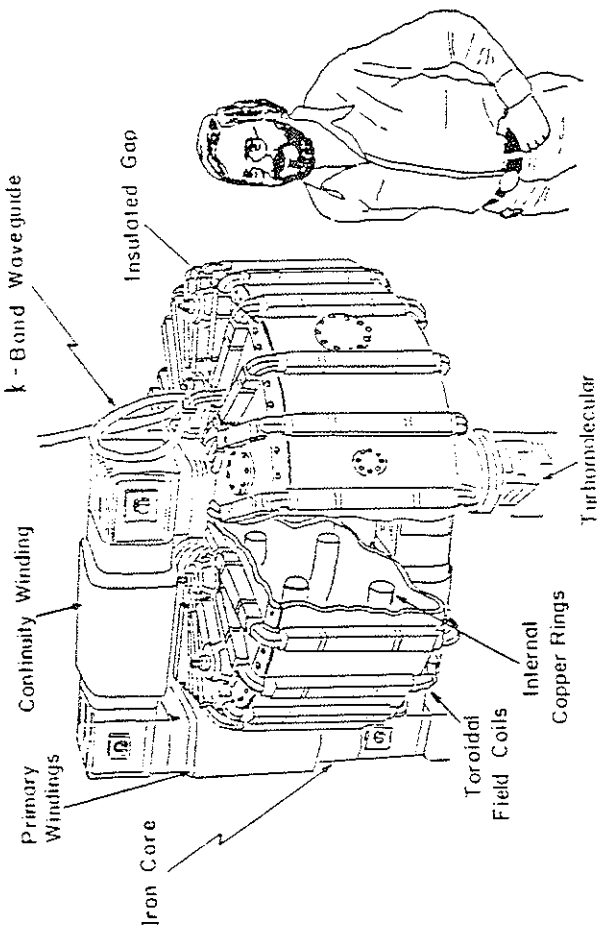

Figure 2-2. Tokapole II dimensions with representative limiter plate shapes. Dimensions are in cm.



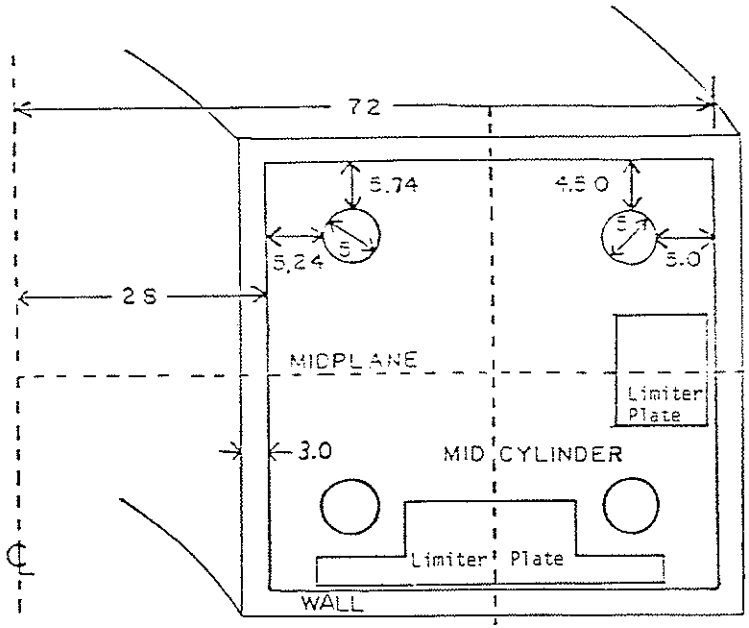

called the common flux as it encircles all four conductors and the plasma. Each divertor and the plasma has a private flux region. A four-null separatrix divides these regions (Figure 2-3).

The toroidal field, $B_t$, is produced by 24 sets of four wires. The wires cross the toroidal gap at uniform intervals to minimize field errors. Image currents driven in the conducting wall compensate for the spacing of the windings and improve the uniformity of the $B_t$. The toroidal field is driven by a 52 mF, 5 kV (650 kJ) capacitor bank and is passively crowbarred. The half-period is 10 ms.

A typical Tokapole II shot begins with the triggering of a Veeco, piezoelectric puff valve. A 10.6 ms delay allows the gas to spread uniformly around the torus. The toroidal field is pulsed, and 5.7 ms later microwaves are injected to preionize the fill gas. Five hundred microseconds pass before the transformer primary is triggered. The divertors and plasma form the secondary. A poloidal magnetic field is generated. The toroidal field peaks and is crowbarred 3-4 ms later. The time sequence is shown in (Figure 2-4).

Magnetohydrodynamics[2] predicts the plasma pressure gradient will be perpendicular to the plasma current density, $J_p$, and the magnetic field, B.



Figure 2-3. A theoretical poloidal magnetic flux plot.

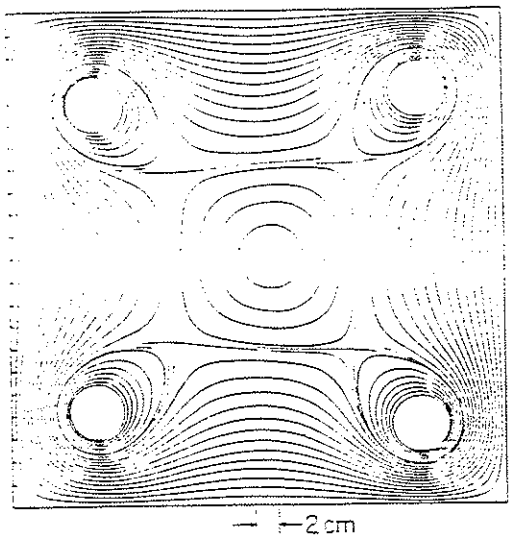




Figure 2-4. Time sequence of a Tokapole II discharge.

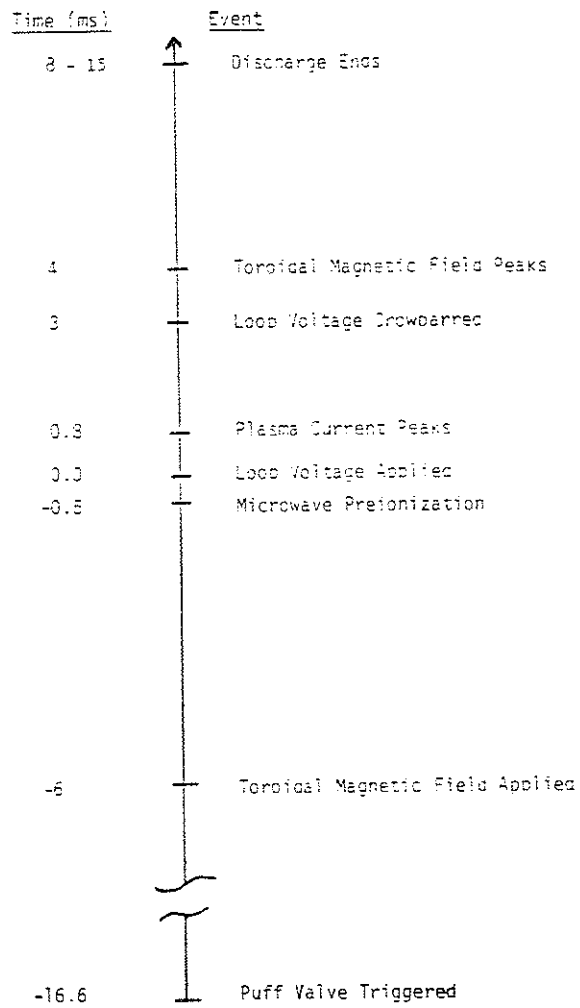




$$\nabla p = J_p \times B \qquad (2.1)$$

Consequently, the helical field lines will trace out nested surfaces of constant pressure. The nested nature of these surfaces is represented by contour plots of the poloidal magnetic flux produced by probe measurements[3] and superimposed on a theoretical plot, like that in Figure 2-3 (Figure 2-5). Presumably a contour plot of the pressure, $p \sim nk(T_e+T_i)$, would give similar results. Here n represents particle density, $T_e$ is the electron temperature and $T_i$ is the ion temperature. A plot of the ion saturation current to a langmuir probe demonstrates this nested nature. The experimental data are superimposed upon a theoretical poloidal flux plot (Figure 2-6). The probe signal is proportional to the product of the electron density and the square root of the temperature. The plot may be considered a first approximation to a plasma pressure profile. The relatively straight vertical contours represent the diverted flux and separatrix region.

Examination of the x-point region yields similar results. Poloidal flux probe measurements thus verify the theoretical plot (Figure 2-7a). Ion saturation current contours also agree with the theoretical flux plot (Figure 2-7b).

Figure 2-5. The plasma current poloidal magnetic flux contours measured by a probe[3] and superimposed on a theoretical flux plot.



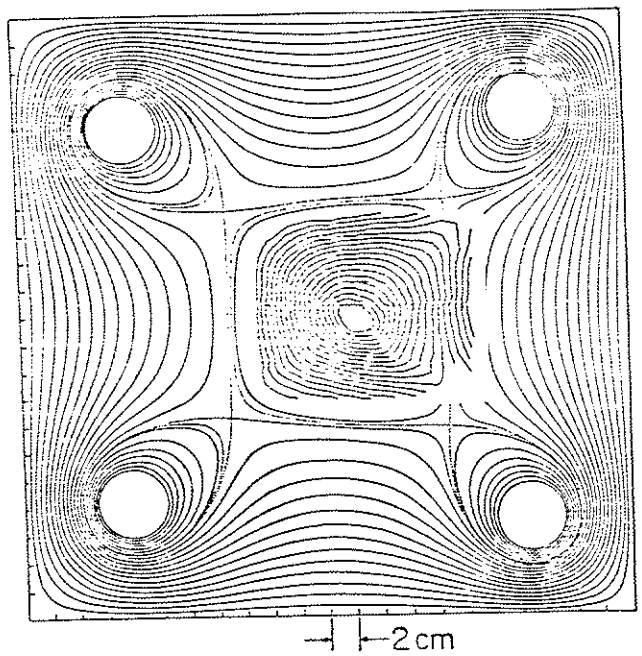

Figure 2-6. Langmuir probe ion saturation current contours of a Tokapole discharge superimposed on a theoretical poloidal magnetic flux plot.



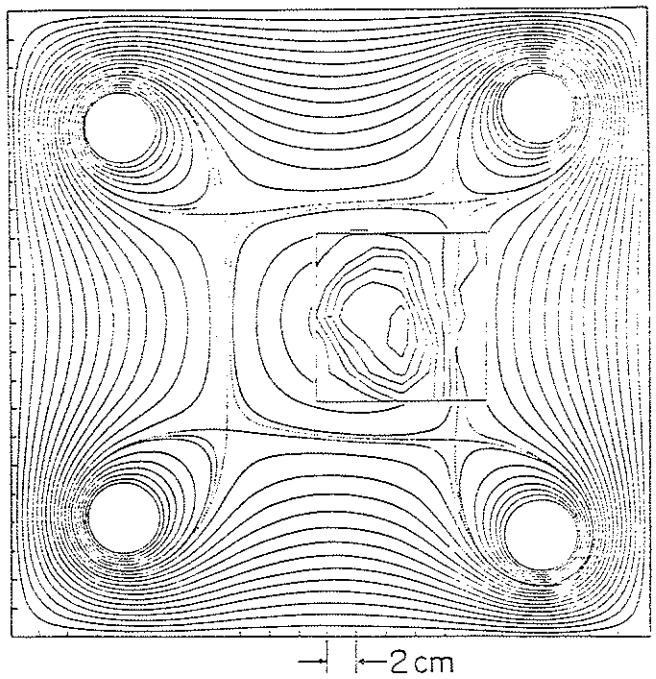

Figure 2-7. Theoretical poloidal magnetic flux contours, with probe measured contours superimposed, near the x-point. (a) Magnetic flux contours. (b) Ion saturation current contours.



a.

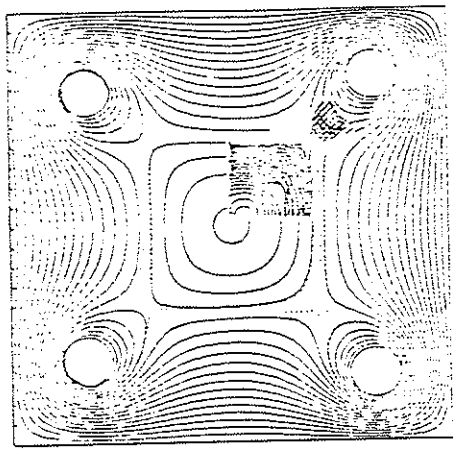

b.

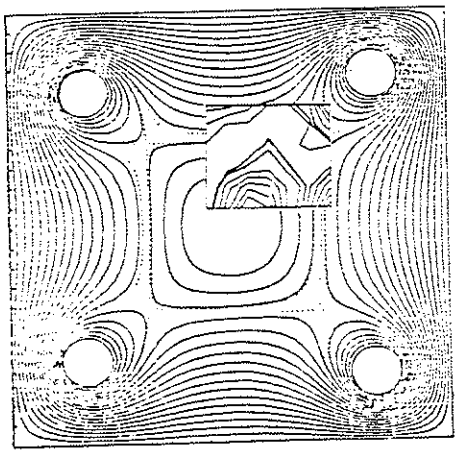

A set of four retractable limiters has been installed, as shown in Figure 2-2. The cross-section of these stainless steel plates intersects the toroidally-directed plasma current. They serve as unpumped neutralizer plates. Presently the plates intersect the diverted plasma and not that in the private flux regions. Liquid-nitrogen-cooled, zeolyte filters have been installed near the piezoelectric puff valves. Glow discharge cleaning with $H_2$ at 50 mtorr and 60 Hz is used nightly. The glow is sustained by an ac voltage between the internal conductors and the walls. A dc offset insures adequate bombardment of the larger wall area. A retractable Titanium getter is also available. An improved pulse discharge cleaning system will be installed by late 1984.

Data aquisition is now handled by a PDP 11/24 with a CAMAC crate of LeCroy 8210, 10 bit digitizers. A TRS-80 model I microcomputer replaced 16 channels of storage scopes for monitoring slowly changing discharge and external circuit parameters.[4] A second TRS-80 with 16 channels has been installed for spectroscopic purposes.

## 2B. Preionization Plasma Sources

The available microwave magnetrons operate in the s, x, and $k_u$ bands. Frequencies of operation are 3, 9, and 15.5 GHz, respectively. The corresponding resonant magnetic fields are



easily computed from 2.8 GHz/kG. A 50 W, cw, s-band source operates during the rise of the toroidal field. This produces a small but useful electron population. The $k_u$-band source provides up to 12 kW for 500 μs and is the primary source for this investigation.

The $k_u$-band pulse has an adjustable length. A set of delay lines serves as a voltage pulse forming network (Figure 2-8). The maximum number of joules extracted from the magnetron is roughly constant. The pulse length and power output is monitored with calibrated diodes through 65 dB of attenuators. The diodes and attenuators were calibrated against a Hewlett Packard 432A power meter.

A second $k_u$-band magnetron is used for several experiments. A less flexible delay line network was available to drive it.

An oscillator built by A.P. Biddle provides second harmonic ICR power to heat a standard tokapole II discharge.[5] About 10 kW of the oscillator's potential output is used to aid startup.

An alternative plasma source has been constructed by A.W. Leonard. A Marshall coaxial plasma gun is now used for refueling and startup studies (Figure 2-9).[6] A stationary supply charges a mobile capacitor bank. The bank is triggered by a spark gap or a class D ignitron. A flexible transmission line carries the voltage (5-15 kV) to the gun which is mounted either

Figure 2-8. Schematic of the magnetron pulsing circuit.



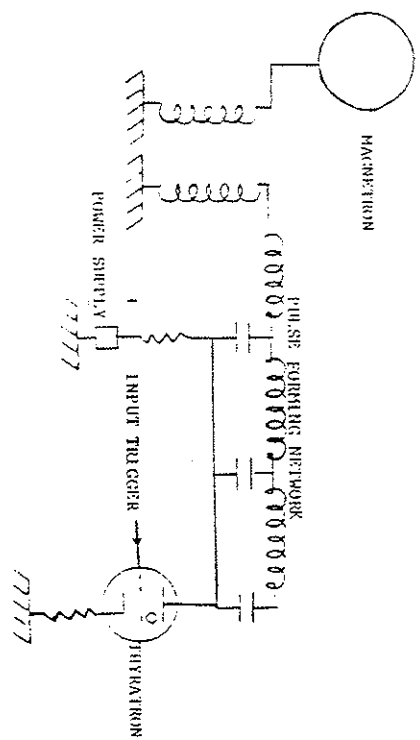

Figure 2-9. Marshall coaxial plasma gun.[7]



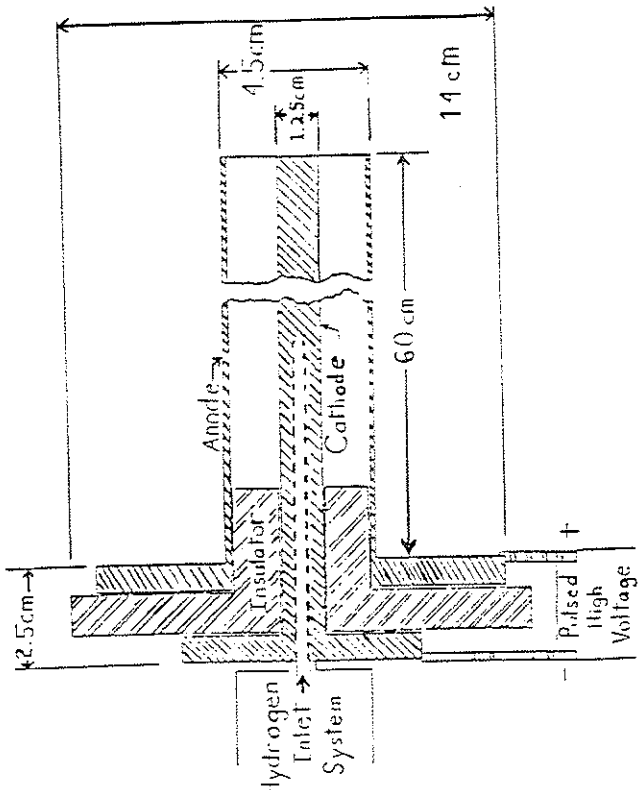

perpendicular or at 30° to the toroidal direction on the midplane.

## 2C. Tokapole II Modifications

The toroidal $V_1$ waveform has undergone major modifications. The original quarter-sine wave now has an overdamped option, which has become the standard (Figure 2-10a). A power-crowbar first option has also been developed. This applies a maximum of 8 V to the poloidal gap until the main poloidal field is pulsed (Figure 2-10b). The main field pulse has a rise time of 300 μs for this option. The rise time results from an inductor installed to protect the crowbar diode stack from the rapid dI/dt when the main field fires. A series resistance was added to damp early and late ringing of the circuit (Figure 2-11). A two-pulse poloidal field option was also developed. The capacitor bank was rewired into two separately triggerable entities. The first pulse was followed by the crowbar and then the second bank pulsed. The option to charge the half banks to different voltages should be operational in late 1984. Many tokamaks use a fast, high voltage bank followed by a sustaining bank at a fraction of the fast bank voltage. This experiment would allow the second bank to be the high voltage one.



Figure 2-10. Toroidal loop voltage waveforms available. (a) Solid line represents the cosine option. Dashed line is the damped option. (b) The power crowbar first alternative. The time delay between the crowbar and the high voltage pulse is adjustible. If the delay was long enough for the total divertor current to reach > 100 kA, discharge breakdown was inhibited.

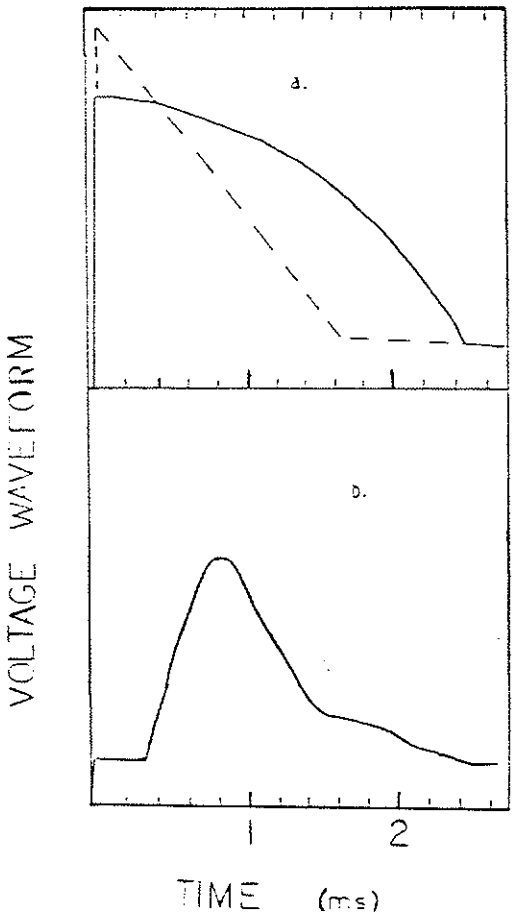




Figure 2-11. Schematic of the circuit options for the voltage waveforms shown in Figure 2-10. The knife switches are remotely operated.

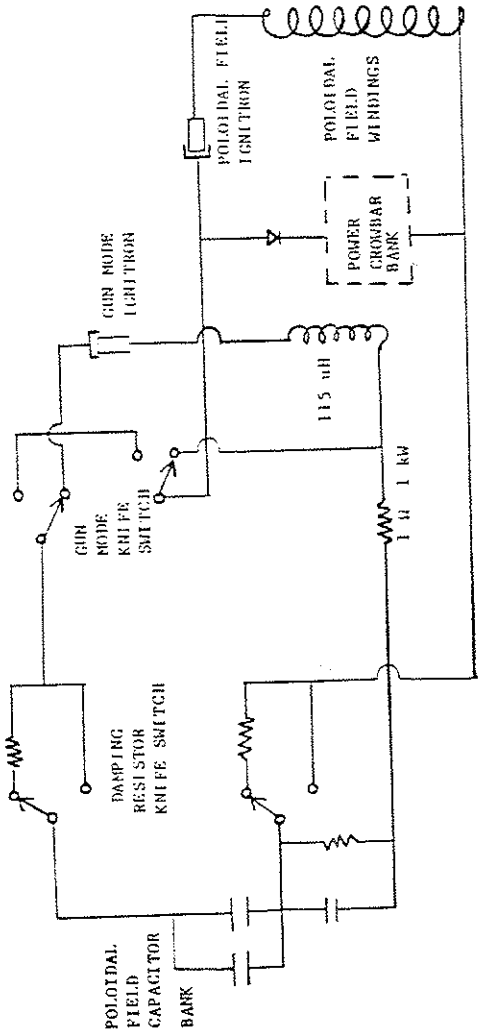




The tokamak discharge has a net expansive force along the major radius. This is due to poloidal field pressure and partly to plasma pressure. Historically, a thick conducting shell was often used to compensate for this motion. Image currents in the shell would result from plasma motion, and a vertical field would result. These image currents decay resistively, limiting their effectiveness. Initial operation of Tokapole II relied on the aluminum vacuum vessel and the poloidal magnetic field of the divertors for plasma positioning. The walls are continued topologically outside the transformer to permit uninterrupted image currents to circulate.

The successor to the thick conducting shell has been an externally generated positioning field (often a set of vertical field coils). The position control is often modified during a discharge by preprogramming or by feedback from magnetic coils sensing the plasma motion. A set of dc vertical field coils has been installed. The coil sets are 80 cm in radius and are located ±30 cm from the midplane. Both coils have ten turns. A welding supply is used to drive up to 300 amps/turn. A variable resistor allows unequal currents in the coil sets. A single coil of 10 turns was wound to produce an axisymmetric field error.

The insulation of the supports of the internal conductors has been modified to allow individual biasing to ± 10 kV. This has allowed some studies of electrostatic boundary effects on the

plasma. The conductors were also exploited as unshielded antennae for the early shear Alfven resonance experiments in Tokapole II.

## 2D. Diagnostics

Tokapole II has a 72 GHz interferometer, for line-average, density measurements. Impurity radiation is monitored by filtered photomultiplier tubes and several grating instruments.[7] An array of seven uncalibrated soft x-ray (SXR) detectors at one side azimuth is supplemented by similar detectors spread toroidally. Similar detectors may be mounted on swiveling probe ports. The SXR detectors are sensitive from 30 to 200 eV photon energies. A hard x-ray (HXR) detector on the midcylinder is sensitive above 1 keV. The vacuum is diagnosed by ion gauges and a residual gas analyzer. The current is deduced by a circuit which monitors the poloidal gap voltage and the primary winding current[4]. A superheterodyne, electron cyclotron second harmonic detector has also been built. A charge exchange analyzer has been used to measure $T_i$.

Apart from these diagnostics, all information comes from probes. The toroidal loop voltage, $V_l$, is measured by a probe consisting of a wire loop. Figure 2-12 schematically demonstrates the operation of this probe. The probe is inserted



Figure 2-12. Representation of the operation of the loop voltage measurement. The probe intercepts a portion of the time-changing flux outside the toroidal loop of interest. When multiplied by a geometric factor, the probe voltage is subtracted from the vertical-cut gap voltage. The gap voltage measures the time changing total flux in the machine. Consequently, the difference is the toroidal loop voltage.

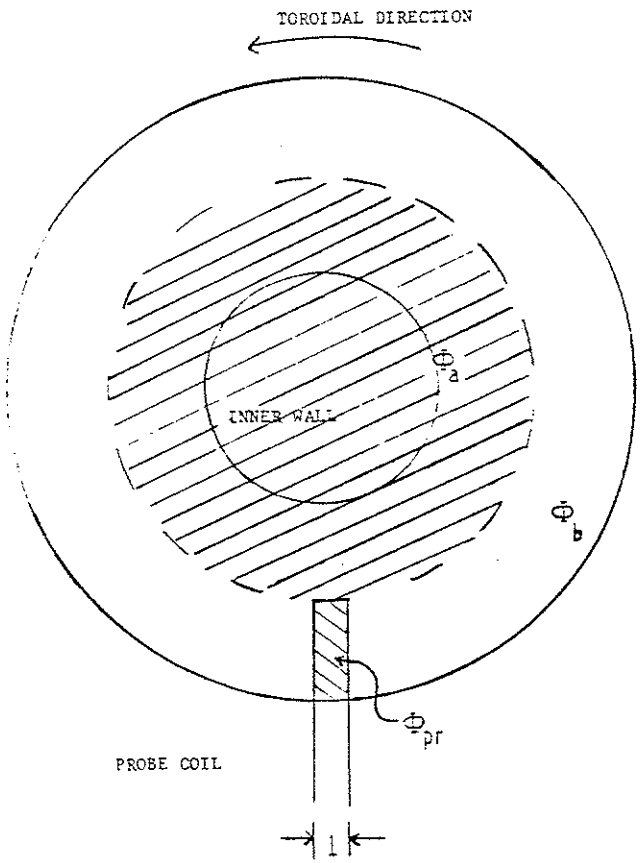




to the center of the machine. The probe voltage, $V_{pr}$, is proportional to the time derivative of the intercepted flux, $d\Phi_{pr}/dt$. The core flux, $\Phi_c$, is the total flux in the machine and is the sum of the flux generating the $V_l$, $\Phi_a$, and the flux outside the voltage loop, $\Phi_b$. The Tokapole gap voltage, at the vertical cut, is the time derivative of $\Phi_c$. Thus,

$$V_{pr} = n \frac{d\Phi_{pr}}{dt} \qquad (2.2)$$

where n is the number of windings in the probe. Thus,

$$\frac{d\Phi_b}{dt} = \frac{c}{l}\frac{d\Phi_{pr}}{dt} \qquad (2.3)$$

where c is the circumference of the voltage loop and l is the length of the wire loop along the voltage loop. The gap voltage is given by

$$V_{gap} = \frac{d\Phi_c}{dt} = \frac{d\Phi_a}{dt} + \frac{d\Phi_b}{dt} \qquad (2.4)$$

or

$$V_l = \frac{d\Phi_a}{dt} = V_{gap} - \frac{cV_{pr}}{l\,n} \qquad (2.5)$$

So measurement of the gap and probe voltages yields the toroidal loop voltage. The design value of the diverted flux without plasma is one half of the core flux and has been verified with this probe. Hence, the plasma will experience roughly half the gap voltage.

Single, double and triple tipped probes[8,9,10] have been used to determine local plasma potential, density, and temperature, respectively. The floating potential, $V_f$, is the voltage across a high impedance termination of the probe. Local density measurements are made with a probe biased into the ion saturation current, $I_s$, region of the current voltage, I-V, characteristic. The expression for ion density, $n_i$, is:

$$n_i = \frac{4I_{si}\left[\pi m_i\right]^{1/2}}{Ae\,(8kT_e)^{1/2}} \qquad (2.6)$$

A is the probe tip area and $m_i$ the ion mass. The formula is valid if $T_i < T_e$. To determine $n_i$ from this one needs $T_e$. A voltage sweep from $I_s$ to electron current saturation traces out the complete I-V plot. The slope at $V_f$ is related to $T_e$:



$$\left(\frac{dI}{dV}\right)_{V_f} = \frac{eI_s}{kT_e} \qquad (2.7)$$

In practice, a triple probe may be used to give $T_e$ without obtaining the I-V characteristic.[10]

$$\frac{kT_e}{e} = \frac{(V_1 - V_2)}{\ln\left(1 + \frac{A_3}{A_1}\right)} \qquad (2.8)$$

The subscripted V and A quantities refer to the bias voltage and area of a tip, ($V_2 = V_f$). The admittance[11] probe has also been used for temperature measurements. The above expression for dI/dV at $V_f$ is the reciprocal for the sheath resistance, $R_s$, of the probe plasma interaction zone. This sheath admittance is measured by a capacitance bridge balanced to read zero with no plasma present. An oscillator drives a sinusoidal waveform with amplitude $\delta V < kT_e/e$ and frequency, f, such that $f < f_{pi}$. $f_{pi}$ is the ion plasma frequency, and this restriction insures resistive rather than reactive response. Circuit response is calibrated against known resistances, and $I_s$ is usually measured simultaneously.

$$\frac{kT_e}{e} = R_s I_s \qquad (2.9)$$

The three temperature measurement techniques agree in the microwave preionization afterglow plasma. While the microwave power is injected, the triple probe gives the most unambiguous and reproducible result.

Small magnetic pick-up coils have been used to map the poloidal flux plot, observe rf resonances in the plasma, and to study magnetic fluctuations. Scintillator probes, provided by Professor R.N. Dexter, have been used to detect high energy electrons. A piece of scintillator plastic is enclosed in the tip of a stainless steel tube. The plastic is shielded from the plasma environment by either the tube wall or an adjustable number of aluminum foil layers. A small rogowski coil, constructed by B. Lipschultz, has been used for current profiles in the diverted region. A retractable rogowski loop which encircles the tokamak flux surfaces has been used to verify the accuracy of the current monitor circuit. A rogowski loop measures current via the magnetic flux passing through its poloidal windings.

$$I = \frac{\phi}{\mu_o NA} \qquad (2.10)$$



Where $\phi$ is the flux through the coil, N the number density and A the area of the turns. A passive integrator attached to the output gives:

$$V = \frac{1}{RC} \int_o^t \frac{d\phi}{dt} dt = \frac{NA\mu_o I}{RC} \qquad (2.11)$$

Note that in regions of the large poloidal field gradients, due to the internal conductors, the baseline of the rogowski signal will be distorted by flux pick up not of toroidal current origin.

Another method of measuring plasma current is the double-tipped saturation probe. The tips are insulated from each other. A differential amplifier with adequate CMRR gives the difference of the saturation currents which is the plasma current.[13]

The probe data below is primarily from the preionization plasma, early startup and edge measurments in the diverted flux. In general for these measurements, $T_e < 60$ eV, and very low current density regions are intercepted. Under these conditions, the probes have little effect on the plasma.

## References for Chapter 2

[1]A.P. Biddle, et al., Nuclear Fusion 19, 1509 (1979).

[2]G. Bateman, MHD Instabilities, The MIT Press, (1978)

[3]B. Lipschultz, Nuclear Fusion 20, 683, (1980).

[4]J.C. Sprott, University of Wisconsin Plasma Studies PLP 889 (1983).

[5]A.P. Biddle and J.C. Sprott, Plasma Physics 23, 679, (1981).

[6]A.W. Leonard, R.N. Dexter, A.G. Kellman, J.C. Sprott, Bull. of the Am. Phys. Soc. 28, 1149 (1983).

[7]R.J. Groebner and R.N. Dexter, Plasma Physics 23, 693 (1981).

[8]F.F. Chen, in Plasma Diagnostic Techniques (R.H. Huddlestone and S.L. Leonard, eds., Academic Press, 1965), Chapter 4.

[9]J.C. Sprott, University of Wisconsin Plasma Studies PLP 88 (1966).



[10]J.F. Etzweiler, Ph.D. Thesis, University of Wisconsin (1977).

[11]J.C. Sprott, Rev. Sci. Instrum. 39 1569 (1968).

[12]D.E. Lencioni, Ph.D. Thesis, University of Wisconsin (1969).

# Chapter Three

## Preionization Plasma in a Toroidal Magnetic Field

Plasma behavior in a purely toroidal magnetic field is crucial to understanding the power balance of an ECR plasma in a tokamak. Other methods of preionization plasma production are subject to the same toroidal physics. Tokapole II results indicate warm electrons, 50 eV $\leq T_e \leq$ 1 keV, dominate the power balance of the ECR plasma, while the microwave power is applied. The existence of the warm electrons is deduced from measurements of a vertical electric field ($E_v \sim T_e/2a$) and of the vertical current due to drifts. The $E_v$ is non-negligible despite the low resistance path provided by the vacuum vessel, contrary to the shorting-out assumption of some authors.[1] The vertical current, due to drifts, is ten times the current anticipated from the bulk ECR plasma. The vertical current losses may account for most of the injected power.

First, the effects of toroidicity on the plasma are briefly discussed. Plasma formation mechanisms and access to resonances are discussed but are not of prime interest to the experiment. A model for the ECR plasma in a purely toroidal field is briefly reviewed. Experiments by other investigators are discussed before Tokapole II results are presented. The approximate power



balance of the microwave-power-on, ECR plasma is presented with reference to the impact on larger devices.

### 3A. Theoretical Considerations

#### 3A1. Effects of a Toroidal Magnetic Field on a Preionization Plasma

The single particle drifts of a plasma in a toroidal field are derived in standard texts.[2] The 1/R decline of the toroidal field produces drift due to $\nabla B$. The curvature of the toroidal field produces a drift, due to centripetal acceleration. Both drifts result in vertical charge separation of the same sense. A vertical electric field, $E_v$, develops and causes an $E_v \times B_t$ drift radially outwards. This drift is charge independent.

Compactly stated:

$\nabla B$ and Curvature drift:

$$v_d = \frac{m}{q}\left( v_{\parallel}^2 + \left(\frac{1}{2}\right)v_{\perp}^2\right)\frac{R_c \times B}{R^2 B^2} \qquad (3.1.a)$$

For estimates of confinement time, it is convenient to use the curvature drift in the following form:

$$v_c = \frac{2kT_e}{eRB_t} \qquad (3.1.b)$$

where $2kT_e = m_e v_f^2$. Since equation 3.1.b uses $n_e kT_e$ instead of $(3/2)n_e kT_e$, it overestimates purely VB drift (by 25%) and underestimates purely curvature drift (by 30%), but is commonly used in the literature as an estimate of drift from both sources. $v_c$ is termed the curvature drift.

$\underline{E_v \times B \text{ drift:}}$

$$v_e = \frac{E_v \times B}{B^2} \qquad (3.2)$$

A study done before the ISX-B experiment[3] assumed $E_v$ to be small for the power balance. The justification assumes that a 1 mΩ vacuum vessel resistance from the top to the bottom shorts out $E_v$. The vertical current due to drifts is estimated to be 900 Amps for a 250 eV plasma of $3.2 \times 10^{12}$ $cm^{-3}$ density.[1] The estimate assumes uniform $T_e$ and $n_e$ over the volume with curvature drift, such that $v_c = 3.85 \times 10^4$ cm/s. Assuming the vessel resistance limits the vertical voltage, ohm's law gives a vertical voltage of $V_v = 0.9$ V. The vertical distance is 54 cm, and so $E_v = 0.02$ V/cm. The resultant $E_v$ crossed with B = 12 kG gives an insignificant radial velocity (about 170 cm/s).



Another argument against $E_v \times B_t$, as a significant loss channel, is made in reference 4. Assuming the drifts are charging plates of infinite impedance, the vertical electric field is limited by the particle energy. If a particle, drifting towards the plate, is unable to pass through the potential gradient, it will not contribute to the charging process. Thus, Borowski, et al. write the $E_{maximum} \times B$ confinement time as:

$$\tau_E = \left[\frac{(\Delta R_{uh}\, m_i)}{k(T_e + T_i)}\right]^{\frac{1}{2}} \qquad (3.3)^4$$

where $\Delta$, the ECR-UHR separation, is the plasma radial scale length used, $R_{uh}$ is the UHR radius (=R), and $m_i$ is the ion mass. This gives $\tau_E = 4.8$ μs and an $E_v \sim 3 \times 10^2$ V/cm for ISX-B. Roughly 30 times the available ECR power would be needed to sustain the plasma.

Further analysis of both arguments is productive. The vessel resistance method ignores an element of the system, the plasma-sheath resistance. The infinite impedance plate approach gives a maximum $E_v$ independent of boundary conditions. Assume the $\sim 10^2$ V/cm, from the infinite impedance plate method, is the upper limit for the plasma $E_v$. Next, consider the sheath resistance of the plasma in series with the vacuum vessel. This resistance limits the maximum $E_v$ which could be sustained by the

plasma, sheath, and vacuum-vessel system. The following expression describes the sheath resistance of a probe collecting ion saturation current in a plasma[5], but is used to provide an order of magnitude estimate for a metallic boundary of the plasma exposed to a drift current.

$$R_s = \frac{T_e}{j_{oi}A} \qquad (3.4)$$

$R_s$ is the sheath resistance, and $j_{oi}A$ is the ion saturation current density times the area of the collecting surface. Using the vertical current, $I_v$, in place of $I_s$ ($= j_{oi}A$) and Ohm's law ($R_s I_v = 2aE_v$), this argument is equivalent to $E_v \sim T_e/(2a)$, but is expressed in terms of a resistance as an intuitive aid.

Using the ISX-B parameters calculated in reference 1, of $T_e$ = 250 eV and vertical current, $I_v$, equal to 900 Amps, $R_s = 0.28\ \Omega$ and $E_v \sim 5$ V/cm. Thus, the $E_v$ supported by the sheath resistance is less than that calculated from the infinite impedance charging method and is much greater than that with the vacuum vessel resistance limiting the maximum value. A $B_t$ of 13.5 kG implies the $E_v \times B_t$ drift velocity is $3.7 \times 10^4$ cm/s. This is on the order of the curvature drift. This estimate suggests a significant vertical electric field could be sustained. The model of Peng, Borowski, and Kammash is discussed further in section 3A3.



The comparison of these predictions to experiment is presented in sections 3B., for ISX-B, and 3C., for Tokapole II.

### 3A2. Accessibility and Coupling of ECRF to the Preionization Plasma

Any startup plasma will be subjected to the above toroidal effects. In the case of ECR generated plasma, accessibility of the interaction region and the coupling mechanism must also be considered.

The propagation of electromagnetic waves through a magnetized plasma is crucial to ECR preionization. Plasma regions which are capable of absorbing the power must be accessible from the launching structure. The first approximation of accessibility comes from cold plasma theory for a slab.[6] The Fourier-Laplace transformed Maxwell's equations give a tensor dispersion relation:

$$\underline{k} \times (\underline{k} \times \underline{E}) + \frac{\omega^2}{c^2} \underline{\underline{\varepsilon}} \cdot \underline{E} = 0 \qquad (3.5)$$

Where $\underline{k}$ is the wave vector, $\underline{E}$ the electric field propagating at frequency, $\omega$, and $\underline{\underline{\varepsilon}}$ is the dielectric tensor. In toroidal geometry, the desired waves propagate perpendicular to the indigenous magnetic field, ($\underline{k} \perp \underline{B}$). For $\underline{E}$ perpendicular

(parallel) to $\underline{B}_t$ the wave is termed extraordinary, X, (Ordinary,O).

The indicies of refraction for perpendicular incidence of the X and O modes may be written:

$$n_O = 1 - \Pi^2 \qquad (3.6)$$

$$n_X = 1 - \Pi^2 \frac{1 - \Pi^2 - \Omega_+\Omega_-}{(1 - \Omega_-^2)(1 - \Omega_+^2) - \Omega_-\Omega_+} = 2\frac{K_r K_l}{K_r + K_l} \qquad (3.7)$$

The K's are components of the dielectric tensor in a rotating coordinate system. $K_r$ ($K_l$) gives the cutoff condition for a right (left) circularly polarized wave propagating along the magnetic field. The two polarizations of the extraordinary wave satisfy the form of the cutoff conditions of parallel propagation despite the fact of perpendicular propagation. The ratio of the plasma ($\omega_{pe} = (n_e e^2/\varepsilon_o m_e)^{1/2}$) to incident frequency ($\omega_o$) is:

$$\Pi = \frac{\omega_{pe}}{\omega_o} \qquad (3.8)$$

The ratios of the electron and ion cyclotron frequencies ($\omega_{ce,ci} = eB/m_{e,i}$) to the incident frequency are represented by $\Omega_-$ and $\Omega_+$



respectively.

$$\Omega_- = \frac{\omega_{ce}}{\omega_o} \qquad (3.9)$$

$$\Omega_+ = \frac{\omega_{ci}}{\omega_o} \qquad (3.10)$$

Plasma cutoffs occur for zero values of the indicies of refraction, and resonances occur for infinite values.

O-cutoff:

$$\Pi^2 = 1 \qquad (3.11)$$

X-cutoff:

$$\frac{(1 - \Pi^2 - \Omega_-\Omega_+)^2}{(\Omega_- - \Omega_+)^2} = 1 \qquad (3.12)$$

or: $K_r K_l = 0$

X-resonance

$$(1 - \Sigma^2)(1 - \Omega_+^2) - \Pi^2(1 - \Omega_-\Omega_+) = 0 \qquad (3.13)$$

If the ion terms are set to zero the UHR is defined as:

$$\omega_{uh}^2 = \omega_{pe}^2 + \omega_{ce}^2 \qquad (3.14)$$

There is no O-mode resonance in cold plasma theory.

In the toroidal geometry of the tokamak, the magnetic field falls as 1/R, where R is the radius. Thus microwaves launched from the outside of the torus experience increasing $B_t$ as they propagate. Such a field gradient sets limits on the accesibility of resonance zones. Launch from this low field side (LFS) is convenient for mechanical reasons, which include the transformer at the inner wall. The following discussion focuses on LFS launch.

For brevity, the discussion is restricted to microwave (15.5 GHz) propagation from the low field side, through a Tokapole plasma with $n_e > 1 \times 10^{11}$ cm$^{-3}$. At this density the X-mode is cutoff one half wavelength radially out from the ECR. This cyclotron cutoff is shown in the CMA diagram in Figure 3-1[2] as a dashed boundary. The microwaves are launched with arbitrary amounts of O and X modes. The X-mode components are reflected from the plasma towards the outer wall.

The O-mode from the LFS then has two sources. These are the launched microwaves and the O-mode waves created by X-mode reflection from the outer wall. The O-mode is not cutoff as the



Figure 3-1. A Clemmow-Mullaly-Allis diagram showing the right hand (R) cutoff as a dashed line separating the low magnetic field and low density region from the UHR and ECR.

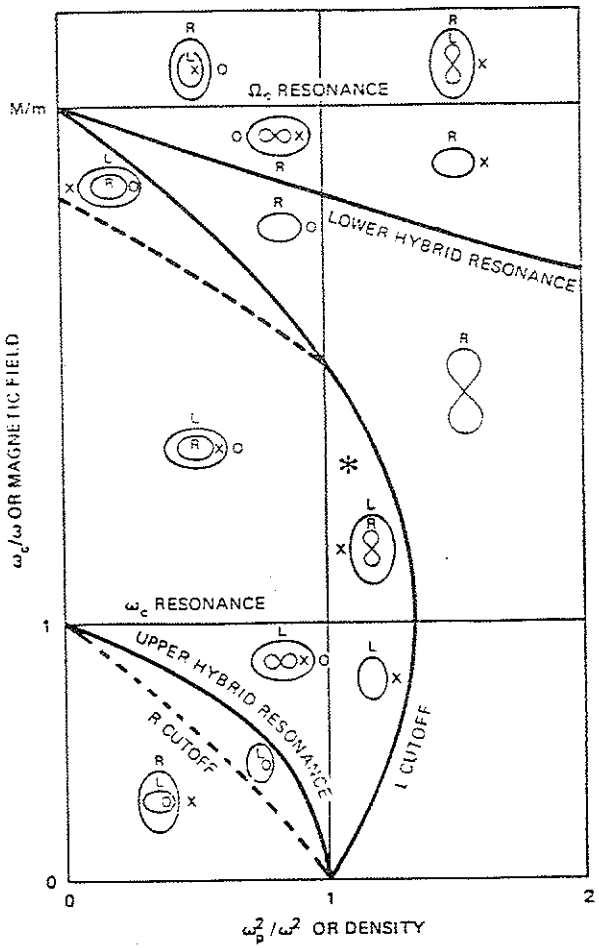




density is not high enough (eq. 3.11). The O-mode which reaches the inner wall is reflected and may convert to an X-mode upon reflection. The portion of the microwave power which is reflected from the inner wall as X-mode radiation propagates freely to the ECR and is absorbed.

The rising plasma density separates the ECR and UHR layers (eq. 3.14), and alters the X-mode polarization to left circular as it propagates from the inner wall. Physically[7], this is due to a polarization of the plasma caused by the finite wavelength of the wave along the axis of the wavevector. The displacement of the electrons with respect to the stationary ions is equal to the gyroradius, $r_g$. The polarization field is twice the applied field and in the opposite direction. The left circular polarization cannot interact at the ECR layer and passes through to the UHR layer.

At the UHR, theory indicates the X-mode converts [8] to an electrostatic plasma wave, the "electron Bernstein mode". The Bernstein wave is absorbed by the electrons, via Landau damping. Mode conversion in addition to ion acoustic waves, has also been observed. [9]

To model experimental results, Anisimov, et al. [10] derive an expression to distinguish the high density regime, with conversion to left circular polarization, from the low density regime. The direction of rotation of the wave field depends on $n_e$, $B_t$, and the angle of propagation with respect to $B_t$, $\alpha$. The condition for wave field rotation change is that $\alpha > \alpha_p$ which is determined by the expressions for the resonance criterion at the cyclotron resonance zone and $\alpha$.[11]

$$\tan^2 \alpha_p = \frac{(1-\Pi^2)(1-\Omega_-^2)}{1-\Pi^2-\Omega_-^2} \qquad (3.15a)$$

$\alpha$ is determined from:

$$\tan^2 \alpha = \frac{1 - u - \cos^2 \alpha_o}{(1 - \frac{u}{2})\cos^2 \alpha_o} \qquad (3.15b)$$

where $\alpha_o$ is the angle of injection and u is defined as:

$$u = -(\Pi^2)(\frac{1}{\omega_- - 1})$$

As the wave propagates towards lower $B_t$, $\alpha$ increases due to an



increase in the perpendicular index of refraction. The result for conversion to the left-handed polarization is written as:

$$\Pi^2 > 2(\Omega_- - 1) \qquad (3.16)$$

Experimentally the left-hand side has the approximate value of 0.04.

Several experiments designed for ECR heating of the ohmically-established plasma launch the X-mode from the inner wall. [12] Heating has also been reported with O-mode launch from the LFS. [13] The former avoid the cyclotron cutoff. The latter is density limited, but within possible reactor parameters. Thus, the same delivery system for heating may be used for preionization.

### 3A3. A Model of the ECR Plasma in a Toroidal Field

A model incorporating the physics issues in sections 3A1 and 3A2 was formulated by Peng et al.[1]. The assumptions of the theory follow the experimental observations of references 9 and 10. The extraordinary mode is launched from the high field side. It is assumed to mode convert to electron Bernstein waves at the UHR, and the power is absorbed in a single pass.

The microwave power is restricted to prohibit the production of runaway electrons. An expression derived in reference 14 is used to estimate the perpendicular electron energy, $W_{\perp R}$, attained near the resonance zone, in the low density regime ($\Pi^2 < 0.04$).

$$W_{\perp R} = 2m_e c^2 \left[\frac{eE_o}{m_e \omega_o c}\right]^{2/3} \quad \text{(eV)} \qquad (3.17)$$

The estimate for ISX-B parameters was 5 keV. For Tokapole the microwave electric field, $E_o$, is 300 V/cm and $\omega_o = 9.7 \times 10^{10}$ Hz, $f_o$=(15.5 GHz). This gives $W_{\perp R} = 3$ keV near the ECR. Scintillator probes detect hot electrons in the Tokapole ECR plasma, which could be in the tail of a distribution function with $T_e \sim 3$ keV.

A particle balance assumes the ISX-B losses are curvature drift, and parallel loss due to field errors, $\delta B$. The authors assume the field error loss velocity ($v_\delta$) is equal to $v_i$ times $\delta B/B$. Comparison to curvature drift velocity gives a criterion for deleterious $\delta B$. If $\delta B > (3)^{1/2}(m_e cv)/eR = (c/eR)(6m_e T_e)^{1/2}$, the error is significant and must be included. They estimate $\delta B > .656$ G is significant and requires correction coils.

The energy balance includes ionization of neutrals, collisions with ions, impurity radiation and the particle losses, but ignores $E_v \times B_t$ drift as discussed in section 3A1. The $\delta B$ chosen was 0.5 G. An estimate of $T_e = 250$ eV near the UHR is obtained, assuming 120 kW injected and $n_e = 3.2 \times 10^{12}$ cm$^{-3}$.



After the particle-energy balance results are obtained, ambipolar electric fields are considered to assist confinement. First, the coldness of the ions causes an ambipolar potential ($\sim T_e/e$) along field lines. Parallel losses are reduced by a factor of the square root of $m_i/m_e$.

The perpendicular confinement assistance is from the sheath at the wall. They assume the magnetic field allows electric field penetration to exceed the Debye length, $10^{-2}$cm. Thus, an $E_{amb} \sim V_{amb} \sim T_e/(ea)$ extends into the plasma and causes an $E_{amb} \times B_t$ drift parallel to the plasma-wall boundary. This drift is poloidal in direction and neutralizes the $E_v$ from $\nabla B$ and curvature drifts. They speculate confinement is improved and impurity influx is reduced by the $E_{amb} \times B_t$ drift. This is in analogy to the streaming of particles along helical field lines when significant plasma current is present. If the 50 eV electrons detected in the UHR layer[3] are responsible for this ambipolar field, the drift velocities would be $\sim 1.4 \times 10^4$ cm/s in ISX-B. This is the same order as the curvature drift, $v_c = 3.85 \times 10^4$ cm/s.

This theory was applied to the Fusion Engineering Device (FED) startup, with modifications due to the experimental results from ISX-B.[4] The ambipolar field drift is a major aid to

confinement, but secondary electrons from hot electron impact at metallic boundaries degrade this extended sheath effect. Using ISX-B data, $T_e \sim 10$ eV, $n_e \sim 3 \times 10^{12}$, and radiated power $\sim 5$ kW out of 80kW imput, the model accounts for 25% of the power input, "Even with secondary electrons". If higher $T_e$ is assumed (UHR layer $T_e < 100$ eV, ECR layer $T_e \sim 20$ eV), the model requires 66 kW compared to the 80kW imput.

### 3B. Experiments on an ECR Plasma in a Toroidal Field

Experiments by Anisimov et al.[9,10,14,15] study the migration of the microwave interaction with the plasma from the ECR to the UHR. The work was done with a device of R = 21.5 cm, a = 6 cm, and $B_t$ = 3 kG on axis. The x-band sources include one essentially cw (0.5 sec) and one pulsed (5-15 μs). Power levels are 1-200 watts and 0.1-10 kW respectively. The microwaves were launched from either the low field or the high field side of the torus. Hydrogen and argon are the working gasses. Pressures range from $10^{-4}$ to $10^{-3}$ torr.

No breakdown is recorded for pressures below $10^{-4}$ torr and/or below powers of 10 watts. The pulsed source launches into a quasi-stationary plasma formed by the low power, cw source. This technique eliminates ambiguities normally present with



drifts. The pulse length is less than the estimated particle lifetime.

At low density, power absorption takes place in the ECR layer. A pressure of $7 \times 10^{-5}$ torr and a power of 50 kW for 150 μs produces x-rays and low frequency oscillations. The gas breaks down, and significant plasma radiation is detected. Microwave fields are detected only up to 40 cm (toroidally) away from injection, after breakdown, implying good absorption. The x-ray energy is 30-40 keV, and the oscillations had a frequency of about 200 kHz. The latter is presumed to be an ion acoustic wave and indicates mode conversion occurs near the UHR. The application of the 15 μs pulse shifts the absorption layer to the UHR, for $\omega_{pe}^2/\omega_o^2 > 0.04$. The density profile was measured with a single Langmuir probe.

The injected electromagnetic wave is assumed to decay into an "oblique plasma wave". This is consistent with the mode conversion discussed in section 3A.. When $\nabla n$ is perpendicular to $\nabla B$, the plasma waves propagate toward higher B. Evidence of fast electron (30-40 keV), generation implies to the authors that Landau damping of the wave is the collisionless power transfer mechanism.

The pulsed source is used to study the radial drift velocity to the outer wall. For $10^{-3}$ torr, the measured outward drift

velocity is $1.3 \times 10^5$ cm/s. The driving mechanism is assumed to be the $\underline{E} \times \underline{B}$ drift.

Holly and Witherspoon [16] used 1-10 kW at 8.8 GHz to study a microwave plasma in Tokapole II's toroidal field. They report the density peak at the ECR layer. The densities of operation, $10^{8}$-$10^{10}$ $cm^{-3}$ separate the ECR and UHR layers by less than 0.5 cm. This is the step size between data points. Also, the toroidal field is changing during the pulse, smearing out the resonance peak spatially.

Experiments on WT-1[17], WT-2[18], Tokapole II[19] and ISX-B[3] report similar observations. ISX-B [3] is unique, as the high power 35 GHz gyrotron has a 15 ms pulse length and launches from the high field side, at 45° with respect to a major radius line of sight. Interferometer measurements and high speed movies demonstrate initial plasma forms at the ECR (97 cm) layer and migrates to the UHR (108 cm) layer after 2 ms. An equilibrium between power in and out is established at 5 ms into the pulse. The resonance zone is smeared out between the UHR and ECR layers. Measurements of $T_e$ confirm this picture. The plasma reaches $5 \times 10^{12}$ $cm^{-3}$ at a bulk $T_e$ of 10 eV. An electrostatic particle energy analyzer indicates $T_e \sim 50$ eV in the UHR layer. A pyroelectric detector acts as a total radiometer and indicates the radiated power is less than 10% of that injected. The energy



balance ISX-B is not as anticipated by the theoretical analysis.[1]

A later ISX-B experiment used another gyrotron with 70 kW at 26 GHz.[20] One of the rail limiters was grounded to collect vertical-drift current. Reversal of $B_t$ should change the sign of the current, but an asymmetry exists in the vertical current. The sign changes but so does the magnitude. The explanation given is that a field error exists of the order $\delta B/B_t \sim 1 \times 10^{-3}$. A model using $\delta B/B = 0.15\%$ and curvature drift matches the experiment, but the e-folding time of the afterglow plasma is 10 ms. This e-folding time implies $\delta B/B < 6 \times 10^{-5}$. The model does not include an $\underline{E} \times \underline{B}$ term, as the thermal electrons (10 eV) are assumed to limit the magnitude of $E_v$.

## 3C. ECR Plasma in the Toroidal Magnetic Field of Tokapole II

The power balance deduced from experiment consists of three loss terms: curvature drift, radiation, and ionization. Non-thermal, vertical electric fields and currents are measured with probes. These experiments indicate three electron temperatures are important. Very early in time (< 150 μs), hot electrons (> 10 keV) are produced near the ECR layer, but few are detected at later times. During the density plateau, warm (50 eV < $T_e$ < 1 keV) and bulk electrons ($T_e$ < 10 eV) may explain the power balance. The warm electrons are suggested by the measured $E_v$ ~ 10 V/cm (~$T_e$(warm)/2a), the ~ 50 Amps of vertical current, and the $T_e$ measured by a triple probe.

The qualitative behavior of the microwave plasma will be discussed first. Quantitative measurements will be presented, as the basis for section 3C6 dealing with the energy balance. The afterglow plasma decays as expected from drifts and was found sufficient for high density preionization benefits (Chapter Four). Attempts to increase the energy confinement time of the ECR plasma were made.

### 3C1. An Overview of the Behaviour of the ECR Plasma



The representative microwave pulse, shown in Figure 3-2, is 300 μs long. The earliest signature of the microwave power, $P_\mu$, absorption is a burst of high energy electrons. These are detected with foil-covered scintillator probes. This signature declines as the Hβ, $n_e$, and impurity radiation increase.

A large, vertical floating potential gradient, $\nabla V_f$, is observed, with probes, throughout the plasma lifetime. Initially this gradient is about 40 V/cm. As the density rises, the vertical electric field, $E_v$, declines and levels off until the $P_\mu$ decays. The plateau value is about 10 V/cm. Assuming $E_v$ ~$T_e$/el where l = 40 cm, the electron temperature would be ~400 eV.

A vertical current, $I_v$, exists during this time, due to curvature drift. At the end of the $P_\mu$ pulse, $I_v$ and $E_v$ decay to nearly zero, within 100 μs. The afterglow plasma has a decay time consistent with drift losses.

Data runs were taken with the microwave power sagging 50% during the pulse. These plasmas flattop in density and radiation output. The power sag was reduced to 5-10% for some experiments. Those plasmas show a slight rise in density throughout the pulse. The maximum density at a particular power level was not reached, due to the limited pulse length of the sources. ISX-B reported that a pulse length > 5 ms produced an equilibrium between power in and maximum density.[3]

Figure 3-2. Representative data during a 16.5 GHz microwave pulse.



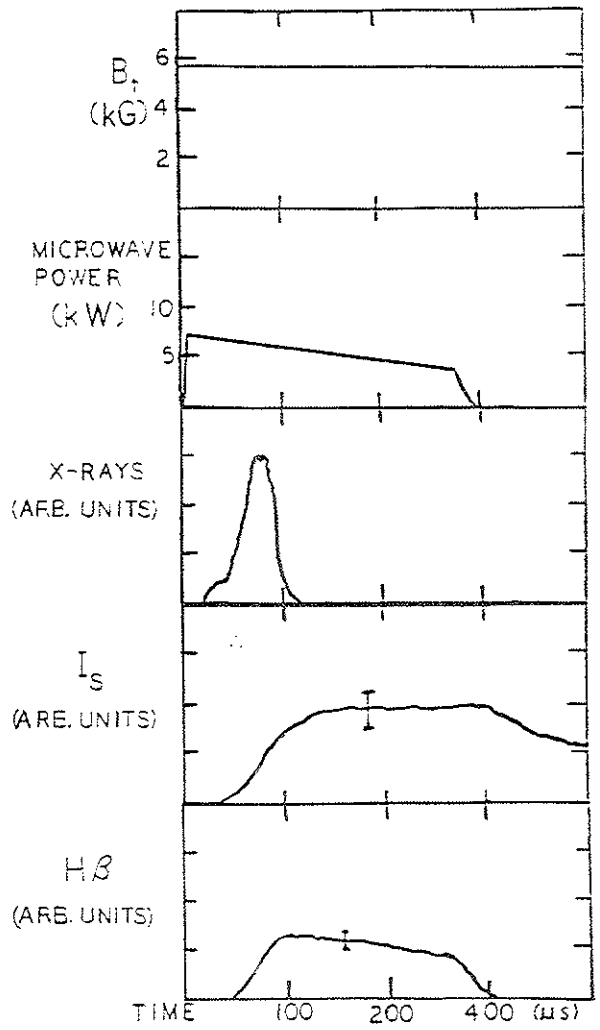

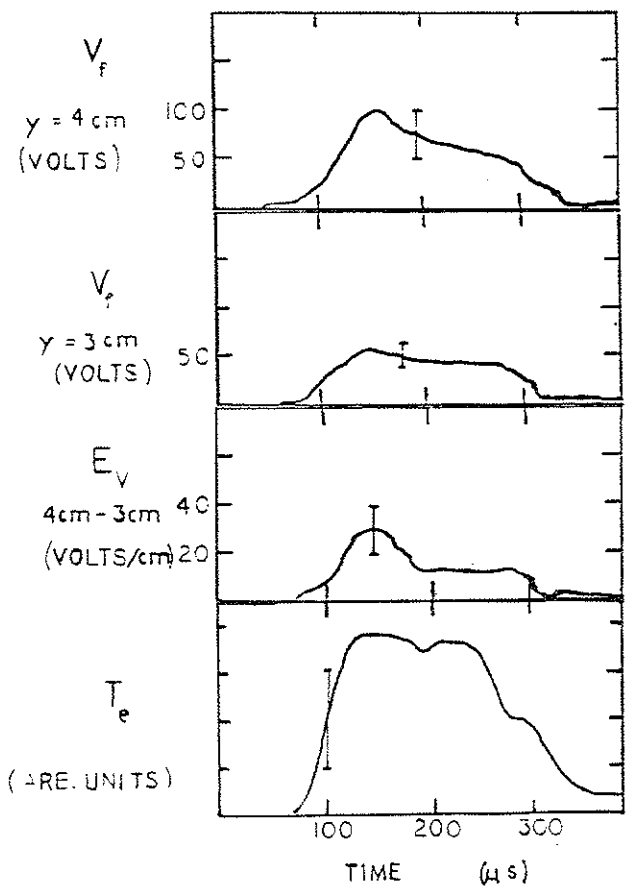




Moderate power (5-12 kW), breakdown was sensitive to pressure. Below 0.50 x $10^{-4}$ torr, a burst of high energy electrons was detected, but little radiation or density developed. A plot (Figure 3-3), of the time-integrated scintillator signal vs. fill pressure is compared to the ion density. The scintillator signal peaks at 0.50 x $10^{-4}$ torr. The density peaked at 2.5 x $10^{-4}$ torr, which was the fill pressure chosen for the following experiments. This corresponds to 1.6 x $10^{13}$ $cm^{-3}$ hydrogen atoms.

### 3C2. Resonance Zone Location

The microwaves are launched from the low field side, and the cyclotron cutoff prevents E-mode penetration to the ECR. This experiment relies on multiple reflections of the sort discussed in section 3A2 to deliver the power to the resonance zone. This is roughly equivalent to launching the waves from the high field side. The conventional wisdom culled from wave theory and previous experiments indicates ECR power from the high field side will initially interact at the ECR layer. As the fill gas is ionized, the interaction at the ECR layer declines. The power passes to the UHR layer, where mode conversion takes place. No modifications are necessary to explain Tokapole II observations.

Figure 3-3. Dependance of $I_s$ (o) and the integral over time of the hard x-ray signal (x) versus fill pressure with 10 kW at 15.5 GHz.



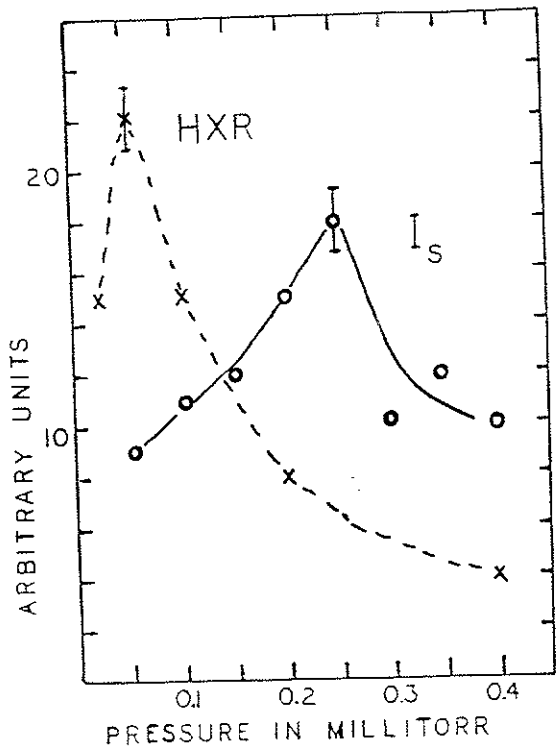

If the ECR layer is positioned beneath a foil-covered scintillator, the first detected interaction, during microwave injection, is a burst of x-rays. These are from hot electrons striking the detector foil. The burst contains electrons up to 100 keV in energy, as they penetrate 1/64" stainless steel. Since the 100 keV signal was very small, the 50 keV electrons observed with the aluminum-foil covered probes were considered in light of the result of eq. 3.16. Assuming a Maxwellian distribution with a particle temperature of 3 keV and $n_e \sim 10^{10}$ $cm^{-3}$, one would expect $6 \times 10^2 cm^{-3}$ electrons at 50 keV. This is consistent with the low density interaction expected, as the detected hot electrons could be the tail of a multi-kilovolt electron distribution function.

Changing values of $B_t$ from shot-to-shot sweeps the ECR layer past a scintillator and filtered photomultiplier tubes on the midcylinder. The x-ray signal, Hβ, and impurity radiation are monitored during the sweep. An $I_s$ radial profile was done, by moving the probe shot to shot.

An estimate of the ECR to UHR separation may be made using eq. 3.14. The measured $n_e = 4 \times 10^{11}$ $cm^{-3}$ for this data run gives the UHR-ECR separation as 3 cm. This involves a shift from 5.5 to 5.1 kG.



Figure 3-4 displays the x-ray signal at 50 μs versus $B_t$. The ECR layer for the 15.5 GHz microwaves would be 5.5 kG. The peak x-ray signal is at the ECR layer. The Hβ signals recorded at 100 and 200 μs peak at lower $B_t$ values, the latter at about 5.1 kG. The shift of the Hβ peak relative to the x-ray peak is related to the transition from the ECR interaction to the UHR, as seen in the ISX-B movies of visible radiation.[3]

The radial $I_s$ profiles migrate with increasing density (Figure 3-5). The shift of 4 cm of the 11.5 kW-$I_s$-rising edge is an indication of the shift of the interaction zone and is within the error of the $B_t$ measurement. At roughly the same parameters, except for density, the 4.6 kW profile is peaked towards the ECR layer. The separation of the ECR and UHR regions at $n_e \sim 1 \times 10^{11}$ $cm^{-3}$ is about 0.8 cm, which is less than the step size of the measurement. As anticipated, the radial migration of the $I_s$ peak is density dependent.

The width of the $I_s$ peak may be explained by the presence of the $\underline{E}_v \times \underline{B}_t$ drift. The plasma would be transported radially by that drift.

The $T_e$ radial profile, as measured by a triple probe during the microwave pulse, has a uniform 50 eV value from the UHR layer across the tokamak channel (Figure 3-6). The triple probe may overestimate the bulk $T_e$ due to a non-Maxwellian electron distribution. The 10 eV value of $T_e$, during the microwave pulse,

Figure 3-4. X-rays and Hβ profiles versus toroidal field. The x-ray peak (x) occurs at 5.6 kG early in time, 50 μs. For the 15.5 GHz pulse, this magnetic field is the ECR location. The Hβ peaks at 100 μs (Δ) and 200 μs (•) are to the low field side of the ECR and correspond to power absorption at the UHR. The microwave pulse was 300 μs long.



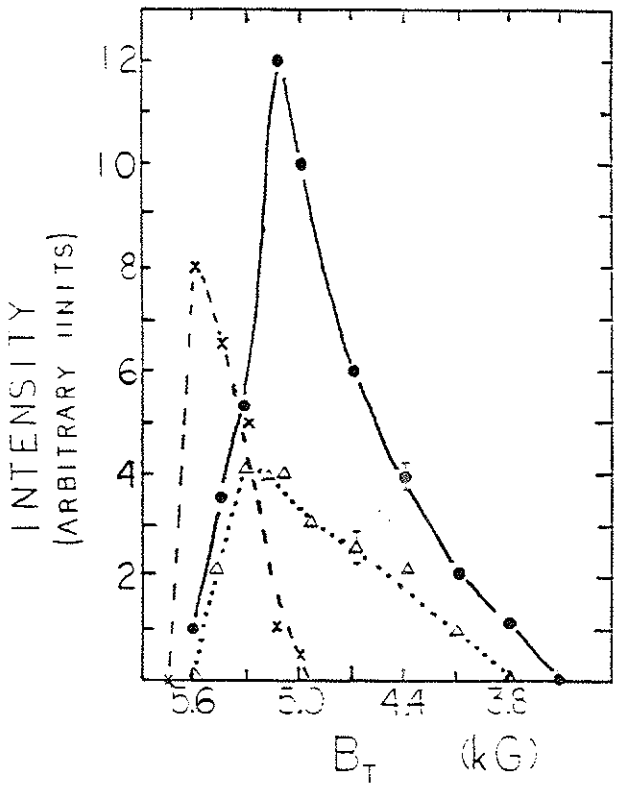

Figure 3-5. Radial ion saturation current profiles. The 4.6 kW (x) plasma at 600 μs is only slightly to the low field side of the ECR (~ -9 cm). The 11.5 kW density peak at 200 μs (Δ) is further to the low field side but represents higher density. The still higher density of the 11.5 kW case at 600 μs (o) is even further out radially. This corresponds to the migration of the interaction region to the UHR as the density rises. The higher the density the further the ECR-UHR separation. The microwave pulses were 600 μs long.



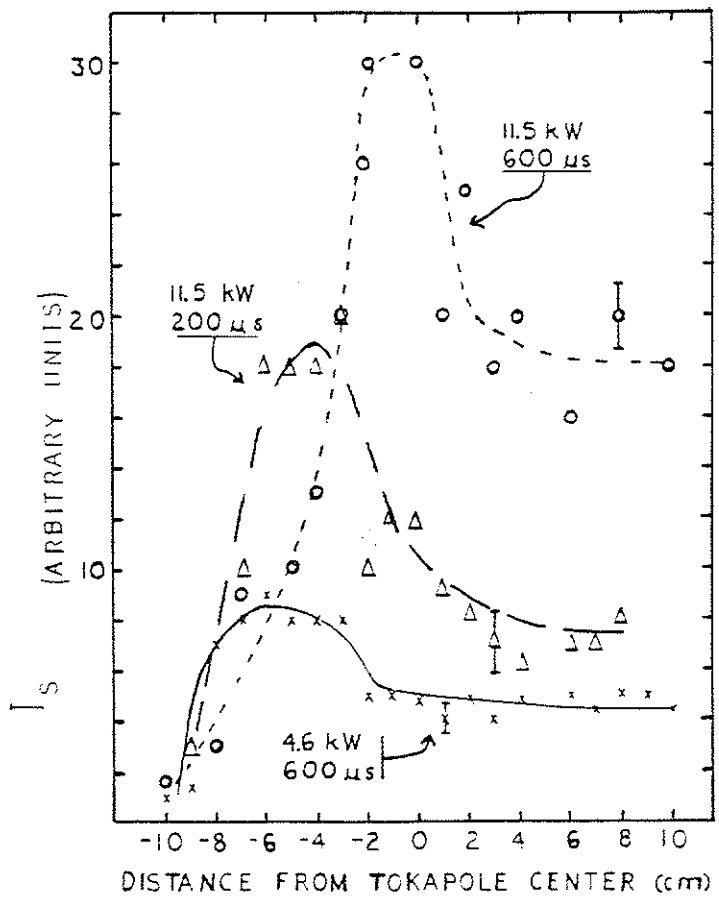

Figure 3-6. Triple probe $T_e$ profiles with the resonance zone at -7 cm. The 15.5 GHz pulse lasted 500 μs. $T_e(r)$, with 4.6 kW of power, is shown for 400 μs (Δ) and 700 μs (x). An 11.5 kW pulse gives a similar triple probe $T_e$ at 400 μs (Δ).



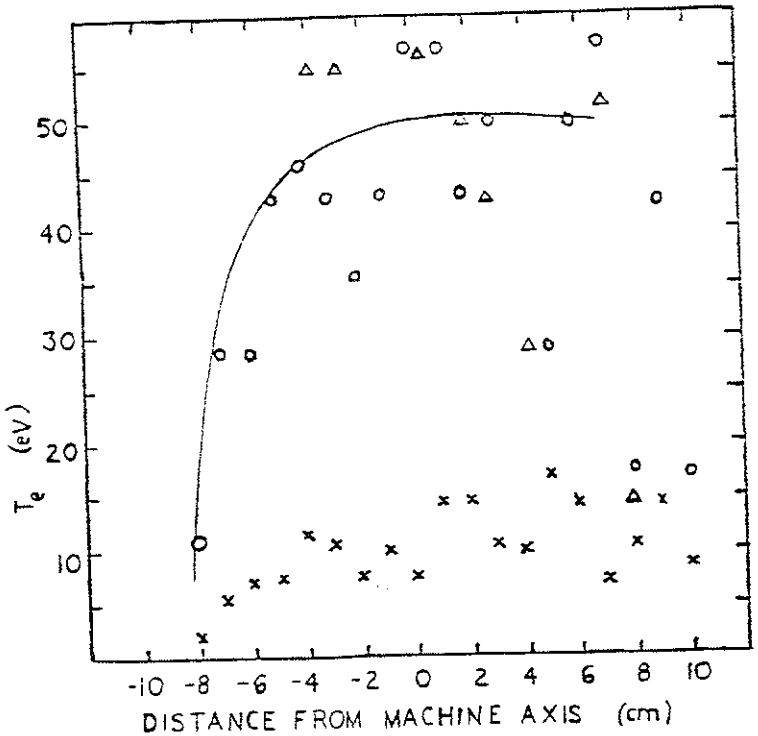

determined from admittance probe measurements will be used as the bulk temperature. After the pulse, triple and admittance probes agree that $T_e \sim 5$ eV. However, the 50 eV measurement compares well with the gridded energy analyzer measurement near the UHR layer of ISX-B, while the 10 eV measurement agrees with the bulk plasma $T_e$ outside the UHR layer[3]. An attempt was made to use a gridded analyzer to determine the electron distribution function during the microwave pulse. This met with failure due to arcing of the grids. The 50 eV value is taken as evidence for a warm electron component which is superimposed on the bulk electron distribution.

In the region between the ECR and UHR, scintillator probes detect hot electrons for the duration of the microwave pulse. A comparison between the signals with one and three foil coverings shows electrons between 50 and 100 keV are present (Figure 3-7 a and b). This is consistent with power deposition by mode conversion, which suggests an electron Bernstein wave is produced and absorbed in that region.

A signature of the warm electrons was measured with floating probes. Both a large $V_f$ and vertical $\nabla V_f$ were observed during the microwave pulse (Figure 3-8). The $V_f$ signal was unreproducible from shot to shot, in the resonance zone. The vertical $\nabla V_f$ was reproducible, usually to within 30%, of the averaged value. About 20 cm from the resonance zone, the $V_f$



Figure 3-7. Scintillator signal in the resonance zones versus time for 1 aluminum foil thickness (---) and 3 foils (-). (a) At low density in the ECR layer, the first 100 μs of the microwave pulse. (b) Near the UHR at the high density plateau.

(a.)

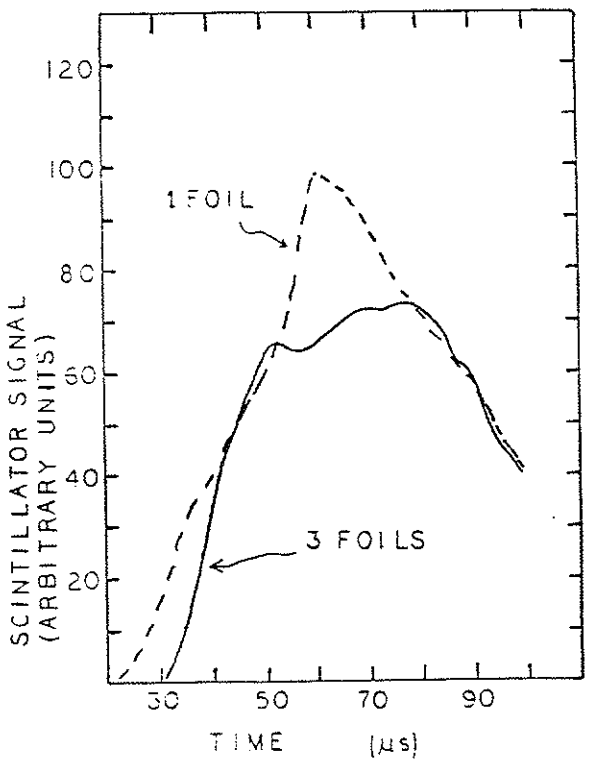
SCINTILLATOR SIGNAL
(ARBITRARY UNITS)
120
100
80
60
40
20
1 FOIL
3 FOILS
30
50
70
90
TIME (μs)



(b.)

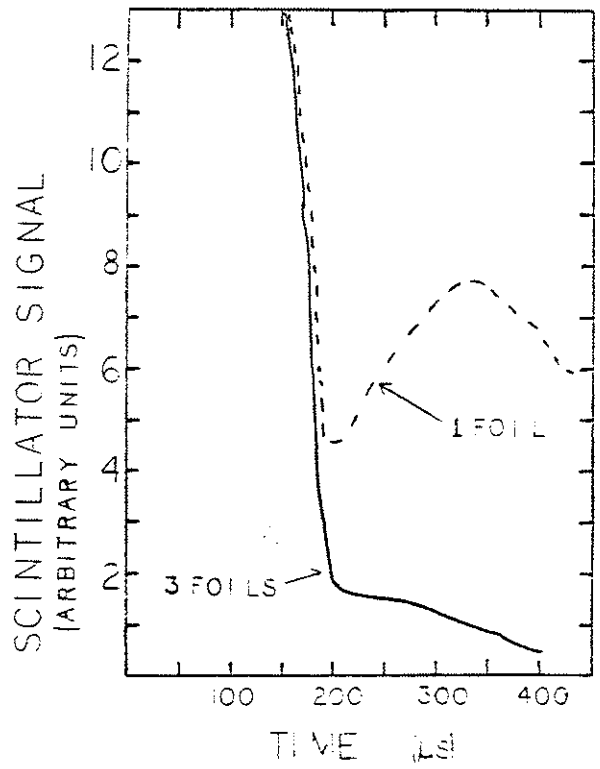
SCINTILLATOR SIGNAL
(ARBITRARY UNITS)
12
10
8
6
4
2
1 FOIL
3 FOILS
100
200
300
400
TIME (μs)

Figure 3-8. (a) The vertical electric field from the difference of floating potential at 13 and 14 cm above the midplane in the midcylinder. The resonance zone for this shot was 8 cm to the high field side of the probe. (b) The corresponding floating potential measured at 14 cm on the same shot as (a). (c) A vertical profile of $V_f$, from shot-to-shot data. The resonance zone was about 20 cm to the high field side of the probe. The shot-to-shot reproducibility of $V_f$ is better outside the resonance zone.



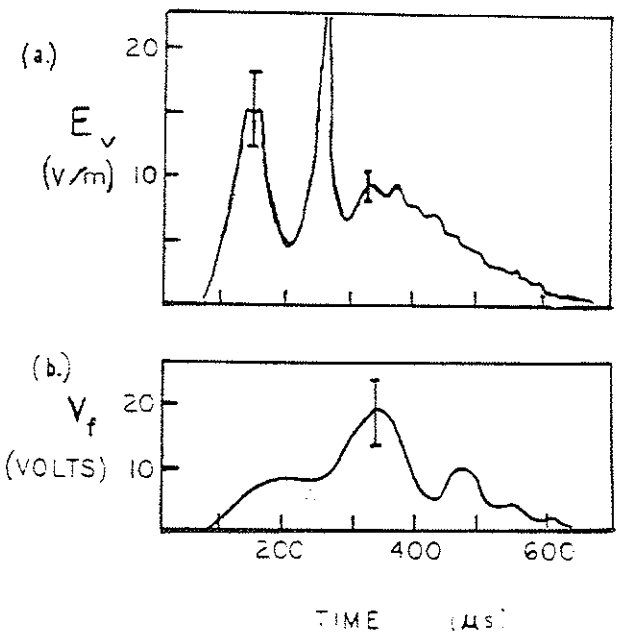

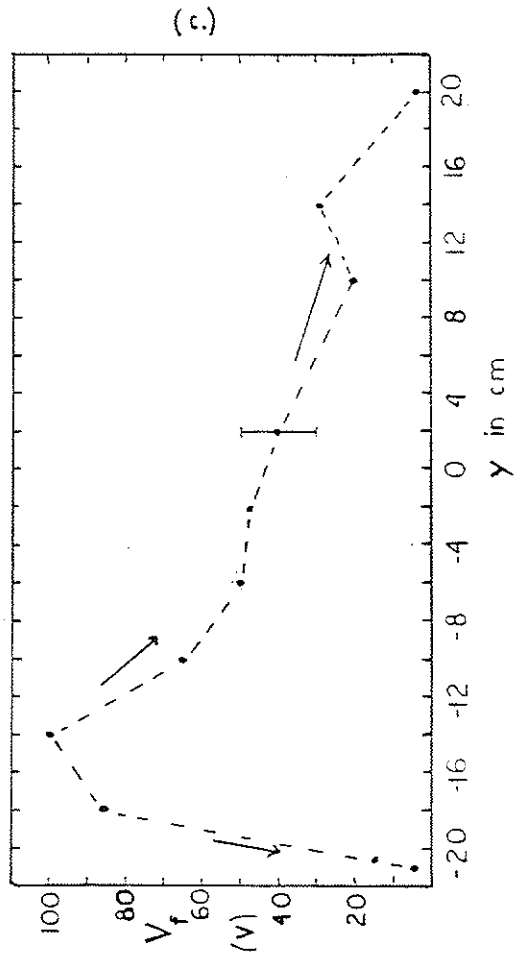




reproducibility was better. Figure 3-8c shows a shot-to-shot vertical profile of $V_f$. The structure is reminiscent of a potential drop diagram around a circuit with the plasma (source of EMF) and the plasma sheath (resistance) at the bottom wall providing most of the drop. The vacuum vessel contributes very little to the voltage drops around the circuit.

### 3C3. $\underline{E}_v \times \underline{B}_t$ Drift Losses

The large vertical gradient in floating potential may be interpreted as a vertical electric field ($E_v$), if $\nabla T_e$ is small, as $V_f = V_p - (3.6)kT_e/e$. $V_p$ is the plasma potential and 3.6 is the appropriate constant for hydrogen. A vertical profile of $T_e$, from an admittance probe, indicates $\nabla T_e < 1$ eV/cm. A series of probes with varying tip separation was used to verify the existence and magnitude of $E_v$. Tip separations of 2 mm, 1 cm, and 3 cm all gave similar values for $E_v$.

When the x-ray burst peaks, the probes indicate $E_v$ is on the order of 40 V/cm in the resonance zone. Rising radiated power and plasma density correspond to a declining $E_v$ magnitude. The density plateau value of $E_v$ is on the order of 10 V/cm. This is a rough average across the plasma. An $E_v$ of ~ 10 V/cm at 5.5 kG implies a radial drift velocity of $1.8 \times 10^5$ cm/s. Figure 3-2 shows the time evolution of $E_v$ with respect to other plasma

parameters. Figure 3-8c shows a vertical $V_f$ profile about 20 cm from the resonance zone towards the LFS. At this distance from the resonance, the gradient is about 3-4 V/cm across the main body of the plasma. Presumably, curvature drift losses have decreased the warm electron population and changed the sheath properties accordingly.

The $E_y$ was also determined by another technique. The afterglow plasma of one microwave source serves as a target for a 150 μs pulse from the second. The $E_y$, measured by probes, at the resonance zone was roughly 10 V/cm, during the second pulse. Ion saturation probes stationed 10 cm apart radially received density pulses which were separated by 30-40 μs (Figure 3-9). The implied radial velocity is 2.5-3.0 x $10^5$ cm/s. Floating potential probe measurements agree with that radial propagation velocity. Anisimov et al.[14] did this experiment, at $10^{-3}$ torr, with a similar result.

These observations imply an E x B drift which is sustained as long as the microwave power is applied. If a population of electrons is supporting an electric field, the magnitude is expected to be $E \sim T_e/2a$. It is plausible that a component of the electron distribution function exists, with $T_e \sim 400$ eV. Discussion of the power balance will indicate that local measurements of $E_y \sim 10$ V/cm may be correct, but plasma loss due to E x B drift is unlikely.



Figure 3-9. Drawings of oscilloscope traces of $I_s$ pulses detected by probes separated by 10 cm radially. When the probes are at the same radius the pulses are simultaneous within the trace width of the scope. The pulse is caused by a 150 μs, 15.5 GHz pulse of microwaves into an afterglow plasma of another source.

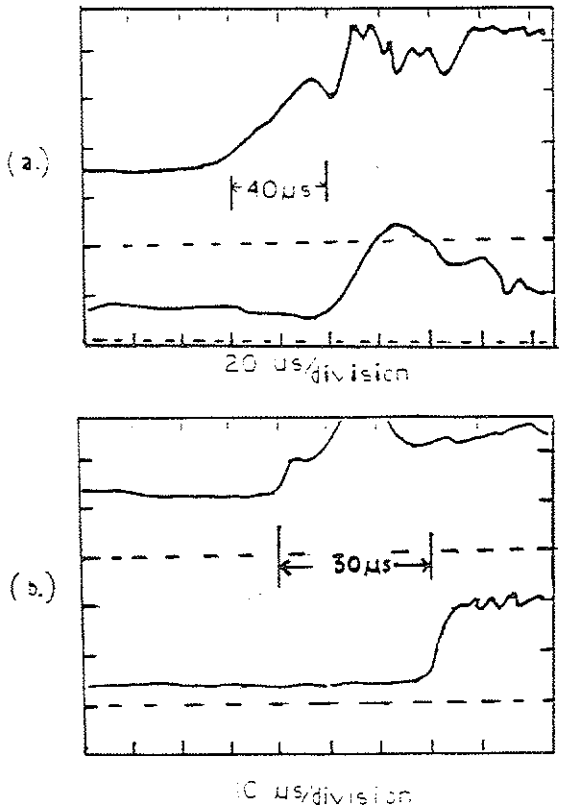




## 3C4. Doping Experiments and Radiated Power

The introduction of impurities into the ECR plasma increases the radiated power and changes the power balance. If the perturbation is significant, other losses might be better understood by the changes in their characteristics. An uncalibrated diode was used as a total radiated power diagnostic. Only relative measurements were made with the diode.

A series of doping experiments was carried out. A hydrogen ECR plasma is produced, while the radiated power, $n_e$, $T_e$, and edge $E_v$ are monitored. Impurity lines and a characteristic line of the dopant are also monitored. The working dopants are helium and oxygen. The percentage puffed in through a Veeco valve is measured by a Bayard-Alpert ion gauge. The ion gauge sensitivity for different gases was taken into account. The ionization potentials of the dopants are 24.5 eV for HeII and 13.5 eV for OII.

To produce a HeII plasma of equal density to the H plasma, 1.8 times more energy is needed. If the line average $n_e$ is within 10%, the two plasmas are assumed to have equivalent densities.

As the helium percentage increases, He II and OIV radiation increase linearly (Figure 3-10). The He-wall interaction desorbs more oxygen, as the small percentage of doubly charged He is

Figure 3-10. Radiation signals versus the percentage of helium replacing hydrogen, in the ECR plasma. $P_{rad}$ is the light sensitive diode signal used as a total radiated power diagnostic. Hβ (x) and O IV (Δ) signals are monitored with filtered pm-tubes.



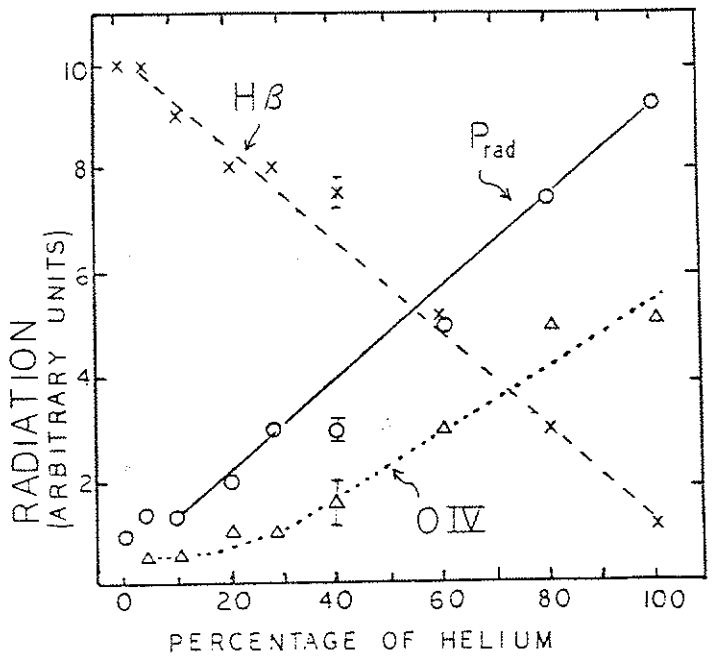

more effective than $H^+$ at releasing impurities from the wall.[21] The 100% helium plasma radiates ten times the power of the hydrogen plasma (Figure 3.10). The bulk temperature and electron density remain roughly constant, but the $\underline{E}_v$ signature declines as the He percentage increases(Figure 3-11.a). The integral of $E_v$ over time was taken as a figure of merit, indicating the presence of warm electrons. At 100% He, almost all the $E_v$ signal occurs before the rise of radiated power.

The behavior of oxygen as a dopant is more complex. A significant amount of power could be consumed in oxygen radiation which was not monitored. The total radiated power increased initially with oxygen percentage, but saturates as $\underline{E}_v$, $T_e$ and $n_e$ decline. The OIV radiation increases by a factor of 20 over the H plasma and a factor of 4 over the He plasma (Figure 3-12). $T_e$ and $E_v$ decline after doping levels reach 5 to 10%. A comparison of the $T_e$ and $E_v$ behavior of the two doping experiments is shown in Figure 3-11.

Both dopants reduce the warm electron signature of the ECR plasma. Helium has little effect on the other parameters, in contrast to $O_2$. A helium plasma requires 1.8 times higher ionization energy and a factor of ten higher radiation output than a hydrogen plasma. The 100% He plasma uses this energy for its formation and radiated power, thereby depleting the warm electron population.



Figure 3-11. The effect of the dopant percentages on $T_e$ and the integral of the vertical electric field signature over time.

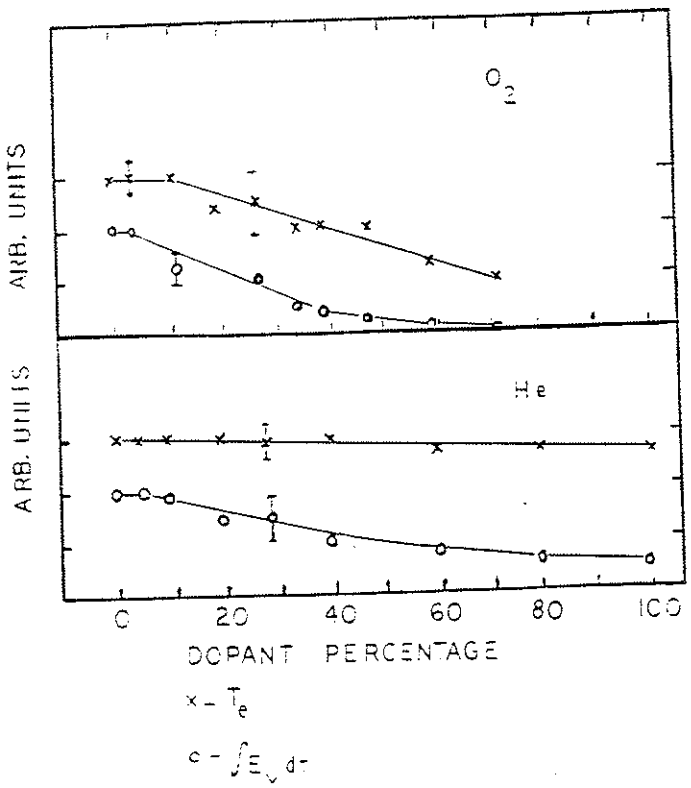




Figure 3-12. Radiation signals versus the percentage of oxygen replacing hydrogen, in the ECR plasma. $P_{rad}$ is the light sensitive diode signal used as a total radiated power diagnostic. Hβ (x) and O IV (Δ) signals are monitored with filtered pm-tubes.

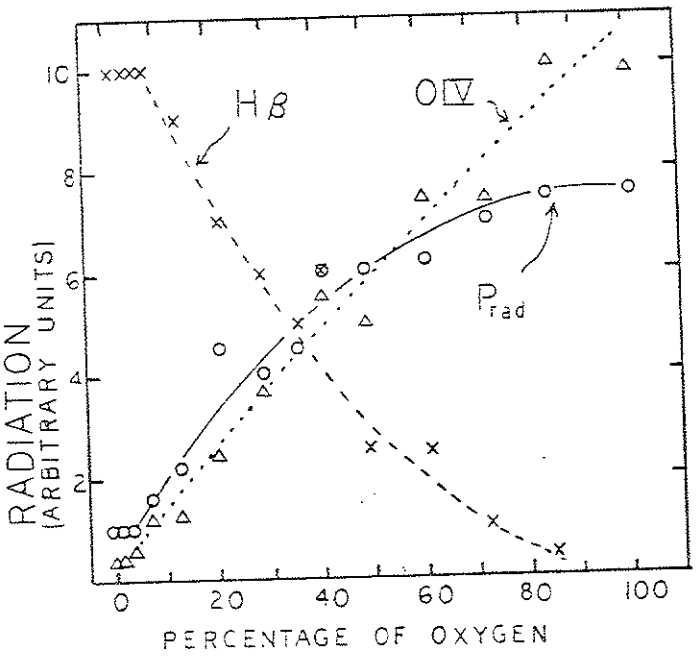




## 3C5. Observations of Vertical Drift Current with and without Impurity Doping

The $\nabla B$ and curvature drifts produce a measurable vertical current, which may be monitored by the current through the internal divertors to ground, $I_d$. The polarity of $I_d$ is reversed when $B_t$ is (Figure 3-13d). $B_t$ reversal causes the ions to drift upwards and the upper divertor collects positive current. The ISX-B experiment reported the current collected by a single limiter varies by a factor of twenty when $B_t$ is reversed. Figure 3-14 is a sketch of their data plot.[20] They lack the signal of a second vertical limiter to compare to. A field error of $\delta B/B \sim 10^{-3}$ for ISX-B was calculated from design considerations and could contribute to the asymmetry. The lack of such an asymmetry in collected current may imply the $B_t$ error in Tokapole II is less than 0.1%.

An $I_s$ probe on the midplane and 22 cm from the resonance zone detects a linear increase in density with ECR power. The $I_v$ collected by the internal divertors also increases linearly with ECR power, as expected as $I_v$ should be proportional to $n_e$ (Figure 3-15). These are the LFS divertors and intersect a cylinder of drifting plasma 24-29 cm from the resonance zone. The linear increase of ion density is expected for this power range and

Figure 3-13. (a) Microwave power in arbitrary units versus time (100 μs/division), for b and c. (b) Upper-inner divertor current to ground in arbitrary units. The toroidal field is in its standard direction, and electron current is collected. (c) Lower-inner divertor current to ground in arbitrary units. The toroidal field is in its standard direction, and ion current is collected. (d) Microwave power in arbitrary units, for e. (e) Lower-inner divertor with standard $B_t$ (top trace), and reversed $B_t$ (lower trace). There is some shot-to-shot variation, but that does not account for all of the asymmetry. Some of the ion current collected may result from the ejection of secondary electrons with ion impacts.



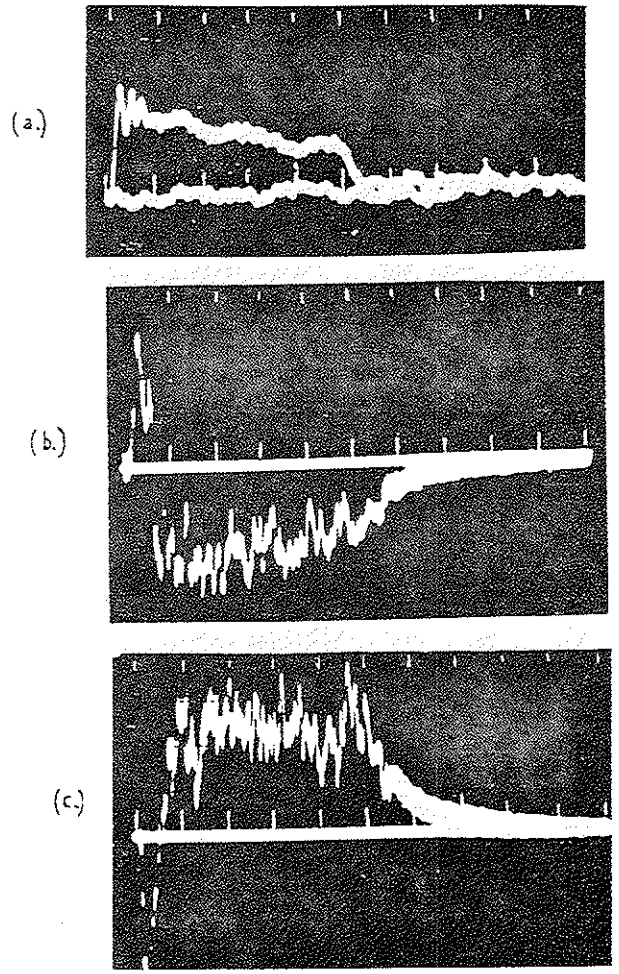

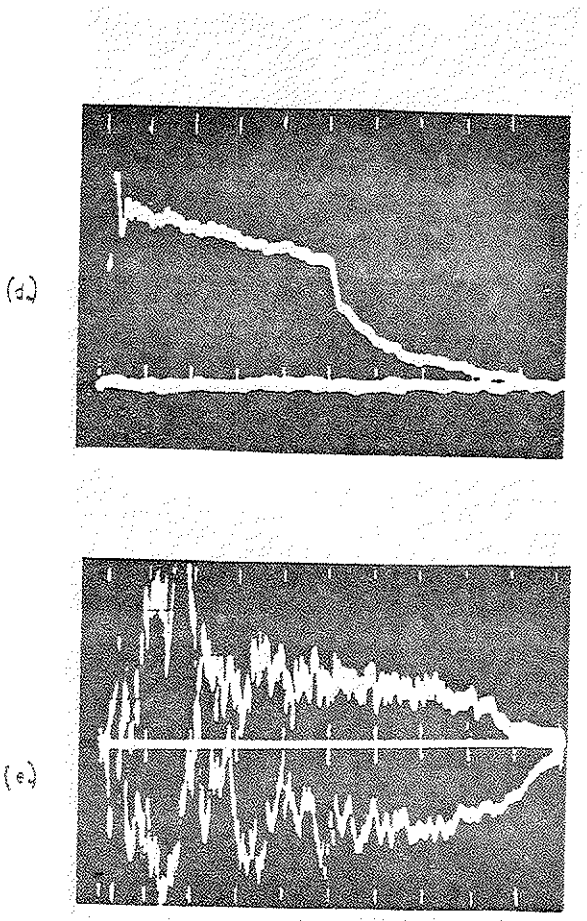




Figure 3-14. A sketch of reference 17's plot of current collected by a grounded limiter with both orientations of ISX-B's toroidal field.

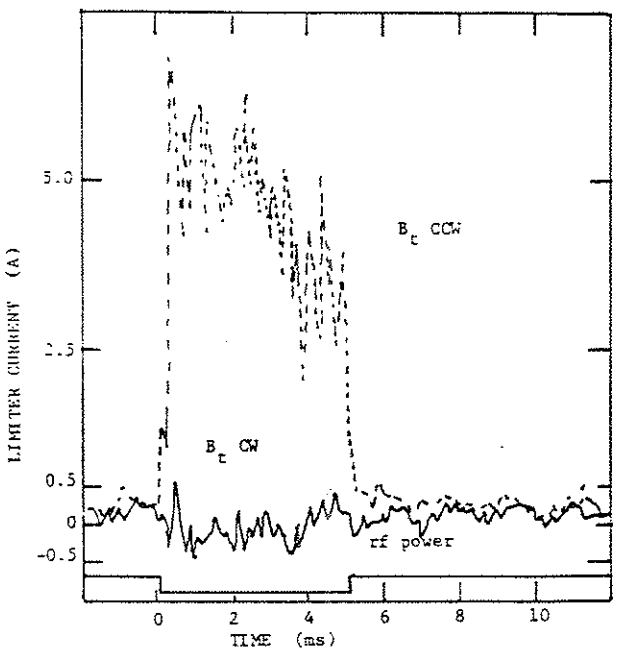




Figure 3-15. Vertical current collected by a grounded divertor, with the resonance zone 20 cm to the high field side of the divertor, versus microwave power. The ion saturation current collected by a probe on the midplane 18 cm from the resonance is also presented versus microwave power measured with calibrated diodes.

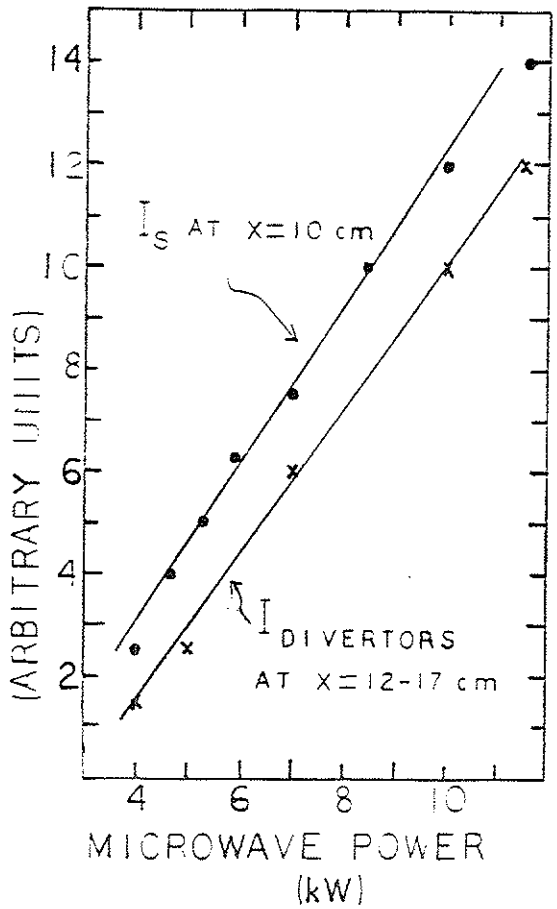




densities below the O-mode cutoff, ~ 3 x $10^{12}$ $cm^{-3}$ at 15.5 GHz (Figure 3-16).

The magnitude of the vertical current may be measured with a double-tipped probe. During the microwave pulse, the entire volume of plasma, to the LFS of the UHR layer, has about the same magnitude of vertical current (Figure 3-17). The $I_v$ decline, when microwave power ends, Figure 3-18, may indicate the warm electron population, which exists during the microwave pulse, carries most of $I_v$.

To isolate the warm electron component of $I_v$, Helium doping was done while monitoring the current through the divertors to ground. Increasing He and consequently radiated power corresponds to a decline in $I_v$ to the divertors (Figure 3-19). A 100% He discharge has little detected vertical current. As reported in section 3C3, the warm electron signature is small when the ECR plasma is 100% He. This is an indication that $I_v$ is predominantly due to the presence of warm electrons.

If the vertical current density is calculated from the current through the divertor to ground divided by the area, the value is > 10 times smaller than that for the split-tipped probe. This may result form the oppositely charged current from the volume between the divertor and the wall, which is absorbed on the other side. Alternatively, a sheath around the divertor may limit the energy of particles reaching the divertor or the sheath

Figure 3-16. Line average density measured by the interferometer versus microwave power measured with calibrated diodes. The error bar is representative of the noise on the scope trace.



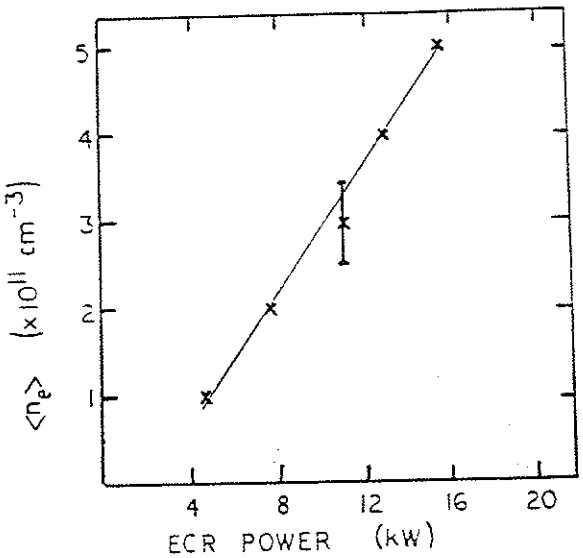

Figure 3-17. The vertical current profile, $I_v$, measured with a split-saturation probe. The ECR would be at -8 cm and the UHR at about -4 cm. Each point is a rough average of several shots. The error bar is representative of the fluctuation range, after deleting probe arcs.



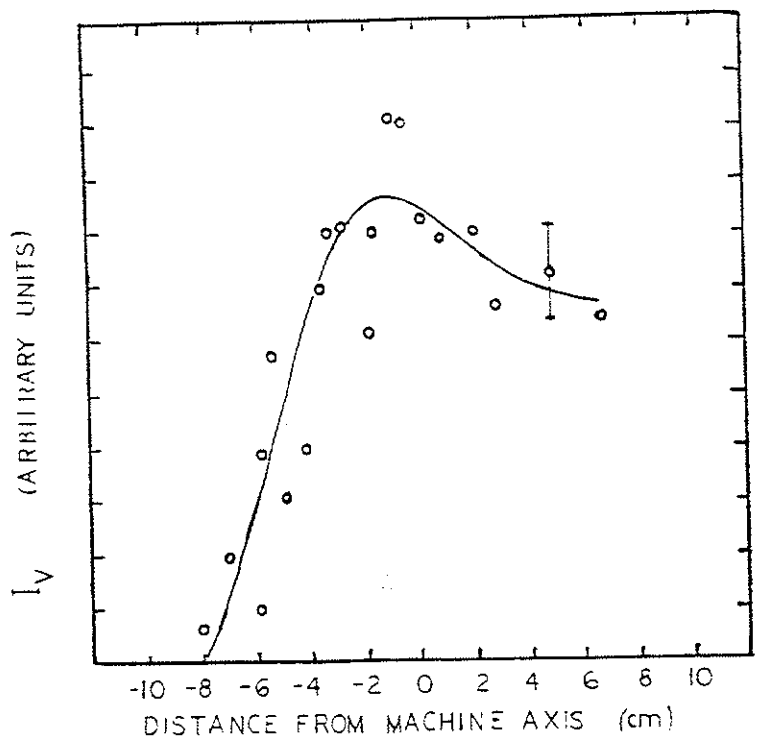

Figure 3-18. The vertical current 10 cm from the resonance zone versus time. The rapid decline corresponds to the end of the microwave pulse.



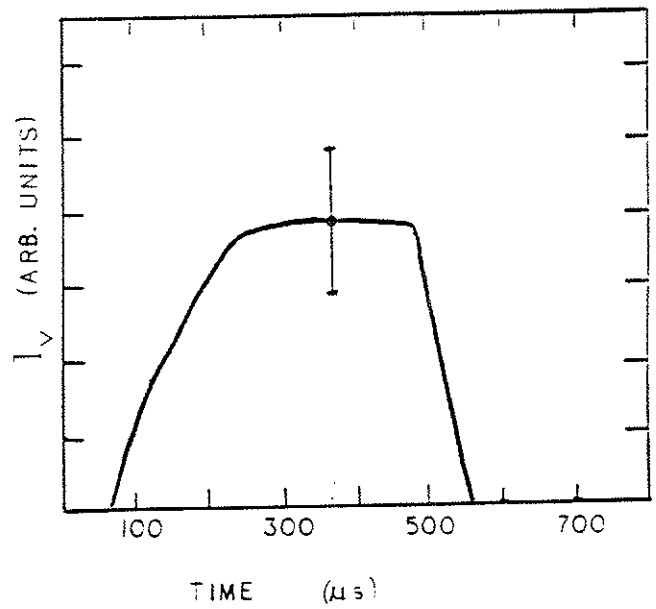

Figure 3-19. Vertical current collected by a divertor in the resonance zone and O III radiation versus the percentage of helium replacing hydrogen in the ECR plasma.



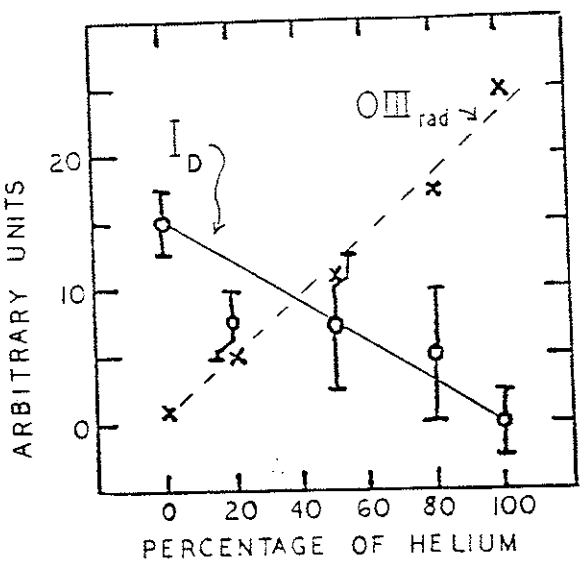

could produce the $E_{amb} \times B_t$ drift suggested by Peng, et al.[1] which could prevent much of the current from reaching the divertor.

### 3C6. An Approximate ECR Plasma Power Balance

The power balance of the ECR plasma during the microwave pulse is examined for $P_\mu = 13$ kW, $T_e = 10$ eV, and $n_e = 4 \times 10^{11} cm^{-3}$. The data discussed above suggest three loss terms: curvature drift ($P_c$), radiation ($P_r$), and ionization ($P_i$). We will assume a steady state situation, so the plasma energy will be constant:

$$\frac{d}{dt}\left[\frac{3}{2} n_e T_e\right] = 0 = P_\mu - P_c - P_r - P_i \qquad (3.17a)$$

This ignores the ion energy and assumes complete absorption of the microwave power ($P_\mu$). Note that the numbers quoted below assume the square cross-section of the vacuum tank, with the resonance zone at a major radius of 44 cm. No detailed particle balance will be discussed.

Equation 3.17a may be rewritten as:



$$P_\mu = \frac{3 n_e T_e}{2 \tau_c} - S_H e_i - P_r \qquad (3.17b)$$

Where $e_i$ is the ionization energy and $S_H$ is the ionization rate. $S_H$ was determined from the radiated power measurement, assuming 60 to 80 eV radiated per ionization.

The power consumed by ionization and radiation of an equivalent helium plasma is as much as 12 times more than in a hydrogen plasma. Considering no other power losses for the He plasma, an upper bound of $P_{rad} \sim 10\%$ of the input power is thus radiated by the hydrogen plasma. This implies an ionization of $1\text{-}2 \times 10^{20}$ particles/s.

The vertical current evidently consists of two parts. A 10 eV plasma, with $n_e \sim 4 \times 10^{11}$ $cm^{-3}$ could account for $I_v \sim 5$ Amps over the plasma volume, assuming curvature drift. The estimated $I_v$ from the split-saturation probe measurements is 50 Amps, which may be an overestimate as the data does not extend to the outer wall. This current is a rough average of measurements across the volume of the tokamak channel. This is consistent with the similar uniformity of $E_v$ ($\sim T_e/2a$) throughout the plasma volume. The hottest electrons are presumably lost vertically in the resonance zone, as they are only detected in the resonance layers with the scintillator probes. A population of warm electrons evidently exists ($T_e > 50$ eV), and is lost more slowly to

vertical drifts. Evidently, the warm electrons smear out over the volume to produce the $E_v$ and 10 times the thermal vertical current density. The 50 Amps of vertical current imply ~3 x $10^{20}$ particles/s are lost. This is evidently an overestimate as suggested above.

Thus, we assume the $I_v$ accounts for nearly all the particle losses. The $E_v \times B_t$ drift would produce too high a particle loss rate, if it swept the plasma volume out with $\tau_E \sim 40$ cm/ 2 x $10^5$ cm/s = 2 x $10^{-4}$ s. Consequently, fluctuations in $E_v$ and/or the $E_{amb} \times B_t$ drift, in the extended sheath proposed by Peng et al.[1], prevent the $E_v \times B_t$ losses indicated by $E_v \sim 10$ V/cm.

If 10 kW of power is lost vertically with 2 x $10^{20}$ particles/s, the average energy per particle would be 300 eV. Thus, the power balance should have a warm electron component. We may write the losses of the vertical current (curvature drift) as:

$$P_c = \frac{3}{2}k\left[\frac{n_{eb}T_{eb}}{\tau_{cb}} + \frac{n_{ew}T_{ew}}{\tau_{cw}}\right]\left[2\pi^2 Ra^2\right] \qquad (3.18)$$

The additional b or w in the subscripts refer to bulk and warm populations. The second term in brackets is the volume. Without detailed knowledge of the



electron distribution function, it is not possible to determine temperature populations.

The curvature drift confinement time, $\tau_c$, is found by dividing the minor radius by $v_c$ from eq. 3.1.b. Preforming some algebra allows 3.19 to be written as:

$$P_c = \frac{6a\pi\left[n_{eb}(kT_{eb})^2 + n_{ew}(kT_{ew})^2\right]}{eB_t} \qquad (3.19)$$

Thus, the power balance for the preionization plasma may be written:

$$P_\mu = \frac{6a\pi\left[n_{eb}(kT_{eb})^2 + n_{ew}(kT_{ew})^2\right]}{eB_t} + eS_{He_i} + P_{rad} \qquad (3.20)$$

We take the ionization rate from the power radiated argument, which assumed 60 to 80 eV radiated for one ionization. Thus, the ionization power is small, $eS_{He_i}$ = 0.2-0.4 kW. $P_{rad}$ is measured to be about 10% of the input power of 13 kW. Presumably the vertical drifts account for the rest of the losses.

For the purpose of scaling to larger machines, ignore $e_i$, $P_{rad}$, and constants, while assuming for constant aspect ratio, $a \sim \ell$, a scale length, $R \sim \ell$, and volume $\sim \ell^3$. This gives:

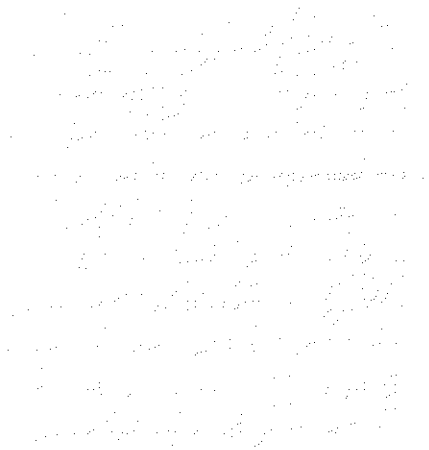

Figure 3-20. The decay of the afterglow plasma. (a) $I_s$ versus time, 0.5 ms/division. (b) $I_s$ versus time, 1.0 ms/division.



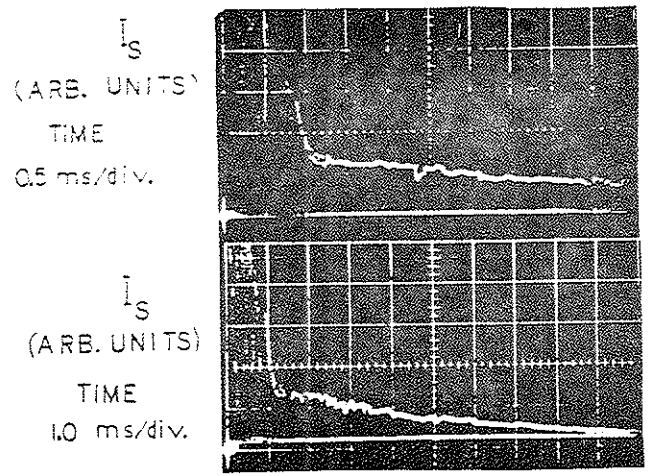

Figure 3-21. Afterglow plasma $T_e$ profiles measured with a triple probe 200 μs after the end of the microwave pulse. (x) - 4.6 kW (o) - 11.5 kW.



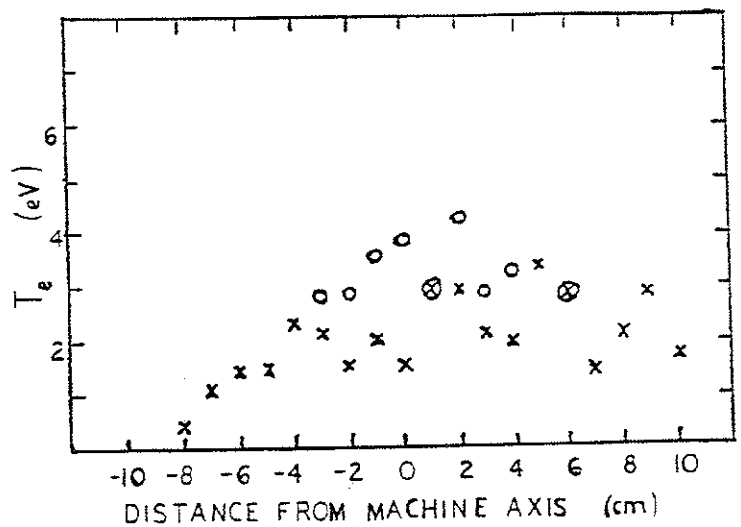

As discussed above the presence of a field error could result in significant losses. Likely sources of such a field error include the primary windings, the transformer, the ohmic heating coils, vertical field positioning coils, and $B_t$ coil misalignment. Some of these would be axisymmetric or nearly so. If such errors were responsible for major power losses, correction fields would increase the efficiency of the preionization plasma production.

Tokapole II is expected to have little stray toroidal field, due to the image currents of the $B_t$ windings in the aluminum shell. To simulate an axisymmetric error field, a single coil was wound at R = 76 cm and 24 cm above the midplane. This coil produces vertical and radial $B_t$ error components in the Tokapole volume.

The single coil error field, $B_{err}$, of about $10^{-3}B_t$ reduces the density across the profile of the preionization plasma (Figure 3-22). The effects of this error coil on breakdown with $V_1$ are discussed in Chapter Four.

The quadrupole-vertical-magnetic-field coils are wound as described in Chapter Two. A field of about $10^{-3}B_t$ depletes the ECR plasma density. No enhancement of preionization plasma density was observed for any selected value of vertical field from these coils. The coils can produce a horizontal field,



Figure 3-22. $I_s$ profiles done shot-to-shot. (o) - with 0.1% toroidal field error provided by a single, ten-turn coil. (x) - no applied error field.

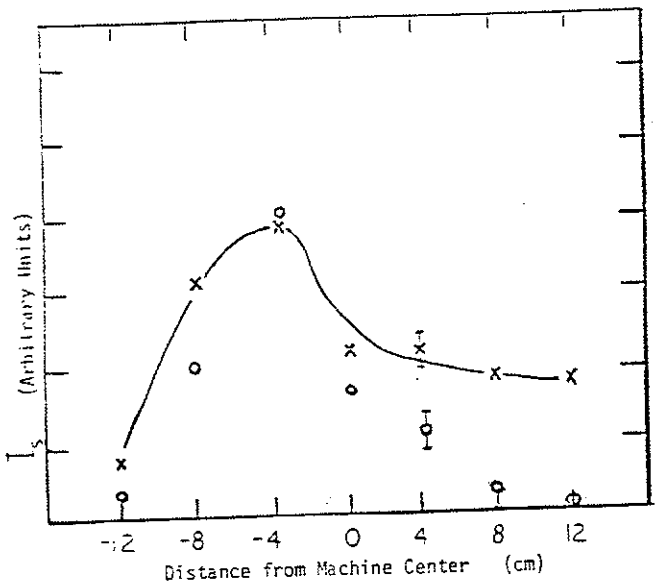




which also failed to show any improvement in the preionization plasma.

The conclusion of this must be carefully contrasted to the other experiments. References 21 and 22 both used the vertical field correction coils to compensate for toroidal field errors, while $V_1$ was applied. No observation of the effects of the correction fields on a plasma in $B_t$ alone were made. However, if a $B_t$ error exists due to a roughly axisymmetric winding misalignment, it should be detected by the experiment above. The observations imply there is no axisymmetric vertical (horizontal) field error, that can be compensated for with simple dc coils, in Tokapole's toroidal field. Such an error of $10^{-3}B_t$ in magnitude was detrimental to ECR plasma density. This supports the conclusion of section 3C4b which contrasted the ISX-B and Tokapole vertical currents due to drift. The $B_t$ reversal experiment, with vertical current, implied a field error of $10^{-3}B_t$ for ISX-B but not for Tokapole.

b. Effects of Bias Voltages Applied to the Internal Conductors

An attempt was made to enhance confinement of the ECRH plasma in the toroidal field with electrostatic biasing of the divertors. Voltages up to 1 kV could be independently applied to each divertor. The applied voltages produce electric fields

perpendicular to $B_t$. This causes an $E_{applied} \times B_t$ drift, which might rotate the plasma poloidally and short out the vertical electric field caused by drifts. This applied field was supposed to do what the $E_{smb}$[12] would, if present.

One might expect the divertors to be screened by the nearby plasma and be invisible to the bulk. The effectiveness of the Debye screening of the biased conductors was not tested, but there were perturbations in the plasma. High frequency noise on the ion saturation signal increases for voltages above ±50 V. The signal amplitude, $I_s$, decreases when applied voltages exceed ±40 V. Presumably, the particle collection of the biased divertors is detrimental, since no benefit was observed. Indeed, the additional electric fields may have enhanced fluctuations and transport. The preionization plasma density profile was depleted, much as in the vertical field case shown in Figure 3-22.



## References for Chapter Three


[1]Y-K.M. Peng, S.K. Borowski, T. Kammash, Nuclear Fusion 18, 1489 (1978).

[2]F.F. Chen, Introduction to Plasma Physics, Plenum Press, (1974).

[3]R.M. Gilgenbach, et al., Nuclear Fusion 21, 319 (1981).

[4]S.K. Borowski, Y-K.M. Peng, T. Kammash,, "RF-Assisted Start-Up in the Fusion Engineering Device (FED)," Oak Ridge National Lab. Rep. ORNL/TM-8319 (1982).

[5]J.C. Sprott, Rev. of Sci. Instr. 39, 1569 (1968).

[6]T.H. Stix, The Theory of Plasma Waves, McGraw Hill, Inc., (1962).

[7]V.V. Alikeav, Yu.N. Dnestrovskii, V.V. Parail, G.V. Pereverzev, Sov. J. Plasma Phys. 3, 127 (1977).

[8]M. Bornatici, R. Cano, O. De Barbieri, F. Engelmann, Nuclear Fusion 23, 1153 (1983).

[9] A.I. Anisimov, N.I. Vingradov, B.P. Poloskin, Sov. Phys. Tech. Phys. 18, 459 (1973).

[10] A.I. Anisimov, N.I. Vingradov, B.P. Poloskin, Sov. Phys. Tech. Phys. 20, 629 (1976).

[11] R.M. Gilgenbach, et al., Phys. Rev. Letters 44, 647 (1980).

[12] V.V. Alikaev, et al., Sov. J. Plasma Phys. 2, 212 (1976).

[13] A. Hakkenberg, M.P.H. Weenik, Physica(N.Y.) 30, 2147 (1964).

[14] A.I. Anisimov, N.I. Vingradov, V.E. Golant, L.P. Pakhomov, Sov. Phys. Tech. Phys. 16, 546 (1971).

[15] A.I. Anisimov, N.I. Vingradov, B.P. Poloskin, Sov. Phys. Tech. Phys. 20, 626 (1976).

[16] D.J. Holly, D.W. Witherspoon, University of Wisconsin Plasma Studies PLP 774 (1978).



[17] T. Cho, et al., Physics Letters 77A, 318 (1980).

[18] Y. Terumichi, et al., in Proceedings of the 24th Topical Conference on RF Heating in Plasmas, University of Texas, Austin, 1981, paper D3.

[19] D.J. Holly, S.C. Prager, D.A. Shepard, J.C. Sprott, Nuclear Fusion 21, 1483 (1981).

[20] A.G. Kulchar, et al., "Preionization and Start-Up in the ISX-B Tokamak Using Electron Cyclotron Heating at 28 GHz," Oak Ridge National Lab. Rep. ORNL/TM-8713 (1983).

[21] T. Somentani, N. Fujisawa, Plasma Physics 20, 1101 (1978).

[22] J.F. Benesch, University of Texas Ph. D. Thesis (1981).

# Chapter Four

## Tokamak Discharge Initiation

There are many ways to provide seed electrons for the breakdown of a tokamak plasma. The methods will be divided into low ($n_e/n_o < 1.0\%$) and high ($n_e/n_o > 1.0\%$) density techniques. When $V_1$ is applied to a low density preionization plasma, the discharge is in the Townsend regime with many generations of primary electrons before breakdown. Either electrons must be provided, or the loop voltage must remain high to achieve breakdown. A signature of this is the delay in the departure of the $V_1$ with plasma from the vacuum value. With high density preionization, the $V_1$ departure from the vacuum value is immediate. This preionization plasma is broken down or has an insignificant number of primary-electron generations to go through to breakdown.

Tokapole II experiments[1] have demonstrated reductions in $V_1$, volt-seconds used for startup, impurity radiation at startup, and runaway electrons. The $V_1$ reduction is successfully modeled by a zero-D code. Volt-second reduction comes from initial low voltage and earlier current rise. Impurity radiation is



evidently reduced by the earlier current formation, which confines the plasma away from the walls and limiters. Runaway electrons are reduced by lower initial voltage and earlier plasma formation, which increases the collision rate and prevents runaway behavior.

A review of discharge initiation experiments follows.

### 4A. A Review of Tokamak Discharge Initiation

#### 4A1. Methods in the Low Density Regime

Discharge initiation studies have evolved steadily. The earliest work focused on the skin effect of the plasma. The time of penetration of magnetic field can be estimated from the ratio of the scale length squared, $l^2$, to the magnetic diffusion coefficient, $D_H \sim \eta/\mu_o$.[2] Using Spitzer resistivity, $\eta = (8.95 \times 10^6/T_e^{3/2})$ $(\Omega\text{-m})$, $l=0.2$ m, and $T_e = 100$ eV, the result is 0.1 s. The 100 eV comes from the radiation-limited temperature at startup. During plasma formation, the transition from hollow to peaked-on-axis profile occurs on a shorter time scale than anticipated. This anomalous skin effect was documented with Thompson scattering in the ST tokamak.[3] Preionization was provided by 100 kHz applied to the gap. At startup, the current was ramped to 30 kA and 30 ms later, to 60 kA. This saved

volt-seconds because the plasma had a moderate $T_e$ and conductivity during the second ramp-up.

Evidence exists from LT-3[4-7] for an m=4 tearing mode as the mechanism for the transition from hollow to peaked-on-axis profiles. Preionization densities of $10^9$ $cm^{-3}$ were attained ($10^{-2}$-$10^{-1}$% of $n_o$) with 10 kW of 2 MHz rf applied 50 μs before $V_l$. A reduction of runaway electrons and a shortening of the pre-breakdown phase resulted. During the current-rise phase of startup, impurity influx was observed. The existence of skin effect with high density preionization is addressed below with the Tokapole results.

A low density regime attempt to breakdown the fill gas away from the wall has been reported, in a toroidal resonant cavity.[8] The goal was to reduce plasma-wall interaction during startup. To do this a high electric field was needed at the center of the vacuum chamber, so a TM cavity mode was excited at 600-700 MHz. Maximum power was 2 kW. The device had a $B_t$ of 0.2 kG and a minor radius of 10 cm. Densities of 5 x $10^8$ $cm^{-3}$ were achieved with a plasma diameter of 10 cm. The time of formation is a few tens of microseconds. Difficulties with excitation techniques and density limits evidently ended this research.

Due to the high toroidal electric field at startup in some experiments, for example LT-3[5], runaway electrons can dominate the current. Runaway rates depend on the toroidal electric field



($E_t$), $n_e$, $n_o$, and $T_e$. Deductions about confinement and equilibrium properties from runaway behavior were made. For example, when runaways are quenched with probes, the early OI radiation falls 20%. Evidently, the thermal-plasma-wall interaction generates most of the early impurities. Reduction of the runaway population is achieved by reducing the toroidal electric field. This reduction is not produced by preionization techniques. The original value of 21 V/m is unusually high for $E_t$ in tokamaks. The reduction to 8 V/m is a normal startup $V_l$ for a tokamak of the size of LT-3. The preionization densities of $10^9$ $cm^{-3}$ did reduce runaways and shorten the pre-breakdown stage.

Confinement is achieved when enough toroidal plasma current is produced to effectively pitch the magnetic field into helices. A rough estimate of this threshold current may be obtained. If the poloidal velocity of a particle due to the poloidal-magnetic-field component exceeds the vertical drift velocity due to toroidal drift, $v_c$, confinement is obtained. Assume cylindrical symmetry and $B_{poloidal}(a) = \mu_0 I/(2\pi a)$. Represent the thermal velocity along field lines as u and the deviation of the field lines as $B_{poloidal}/B_{total}$. Confinement is achieved if:

$$v_c < u\frac{B_{poloidal}}{B_{total}} \qquad (4.1)$$

Then $I_p$ must exceed $u(2\pi ma)/(\mu_0 eR)$, e.g. if $T_e = 100$ eV, then $I_p > 66$ Amps for Tokapole parameters. The LT-3 group estimates I~100 Amps for $T_e \sim 100$ eV. Note this current does not imply any MHD equilibrium, but only the poloidal field necessary to compensate for $v_c$ at a particular parallel-to-$B_t$ velocity.

In lieu of an adequate plasma current, some benefit is derived from a vertical magnetic field perpendicular to the toroidal direction. If $V_\perp$ drives a vertical current along the deviated field lines in the opposite sense to the vertical drift current, confinement is obtained. A threshold value for $B_\perp$ is determined when curvature drift are compensated. The threshold may be determined from the net drift velocity, written as:

$$v = v_c - u\frac{B_\perp}{B_t} \qquad (4.2)$$

Following reference 7, a runaway which is stationary at time $t = 0$ attains a velocity, $u = (e/m)(E_t)t$, at time t. The net drift velocity at a later time is:



$$v(t) = \frac{u^2}{R\Omega_-} - u\frac{B_\perp}{B_t} \qquad (4.3a)$$

or substituting for u:

$$v(t) = \frac{eE_t}{mB}t\left[\frac{E_t}{3R}t - B_\perp\right] \qquad (4.3b).$$

The distance drifted is:

$$d(t) = \frac{eE_t}{mB}t^2\left[\frac{E_t}{3R}t - \frac{B_\perp}{2}\right] \qquad (4.4)$$

The desired result occurs when $v = 0$ and $t = RB_\perp/E_t$. The distance drifted becomes:

$$d = \frac{eR^2B_\perp^3}{6mE_tB} \qquad (4.5a)$$

or

$$B_\perp = \left[\frac{6dmEB}{eR^2}\right]^{\frac{1}{3}} \qquad (4.5b)$$

If d > a (< a) most electrons are lost due to $B_\perp$ (toroidal drifts). For both LT-3 and Tokapole, $B_\perp$ is about $10^{-3}$ T.

Another application of a $B_\perp$ is the correction of axisymmetric $B_t$ errors. For these experiments done on JFT-2[9] and Pretext[10], the applied $V_1$ rises smoothly from zero in a sinusoidal waveform. The superposition of horizontal and vertical correction coils reduces the delay from voltage application to breakdown, $\tau_d$.[9] The reduction of $\tau_d$ indicates better confinement of the electrons which are capable of ionizing the gas. The $V_1$ for breakdown decreases by 30%,[10] with optimized correction fields. This is due to stray field correction.

In Pretext,[10] simultaneous adjustment of the dc horizontal and vertical correction fields gives the minimum $\tau_d$. The applied $V_1$ continues to rise after the deviation from vacuum value. Thus, the "breakdown" voltage is not the maximum voltage applied during the discharge. Standard tokamaks, like Tokapole, have cosine $V_1$ waveforms, and typically the maximum voltage applied is taken as the minimum $V_1$ necessary to achieve a discharge.

Doublet III has 24 windings for shaping the discharge, which can be used as 'correction' coils at startup.[11] Reported breakdown $E_t$ was as low as 0.8 V/m with feedback-controlled-correction fields. The $dI_p/dt$ changed from 7.0 kA/ms (1.33 V/m) to 52.0 kA/ms (5.34 V/m). The former $dI_p/dt$ implies a one-turn $V_1$ of 120 V and consumption of 0.85 V-s, to reach the $I_p$ plateau, 500 kA. The latter implies a one-turn $V_1$ of 480 V and consumption of 0.46 V-s, to reach 500 kA. Volt-seconds are traded for a reduction in $V_1$ in this work.



ICRH has been used for a preionization source on Pretext.[10] The ICRH produces densities of $10^9$ $cm^{-3}$ with 0.3-3 kW at 12 MHz. A loop voltage reduction of ~ 30% is reported with 300 W and remains unaltered up to 3 kW. No measurement of preionization density vs. power is reported. Ionization by energetic ions is assumed to be the preionization mechanism.

No effect on breakdown from biasing the limiter was observed. Thus, the limiter is not acting as a significant source of secondary electrons. Also ionization by ions before the Townsend criterion is met is important to breakdown. Additionally, the application of $V_1$ with small dV/dt is desirable.

### 4A3. High Density Startup Methods

#### a. Startup Experiments Using ECR Preionization

ECR preionization and preheating have been suggested to lower $V_1$ requirements at startup.[12] This work did not include the possibility of current driven by the ECR heating.[13]

Holly and Witherspoon[14] used ECR to preionize ohmic discharges in Tokapole II. They reported 50% reduction of vacuum-ultraviolet-impurity radiation during discharge formation.

Three methods of breakdown were compared in FT-1,[15] including the standard-unassisted technique. Preionization is accomplished by two methods. A $V_1$ spike is applied with opposite polarity to the usual ohmic heating pulse. This reduces the forward $V_1$ needed and reverse-biases the core adding to the available volt-seconds. The other method is ECR preionization. A 2 μs pulse of 30 GHz microwaves is injected from the LFS at 60-70 kW. Both techniques lower the $V_1$ and eliminate HXR's due to runaway electrons at startup. The reverse voltage spike has some disadvantages. The magnitude of the spike retains the insulation problems of standard-high-$V_1$ startup. Stav[11] reports the current due to reverse-bias preionization, inhibits Doublet III low-voltage startup.

Similar results, for ECR preionization, have been reported by other groups.[16-18] The ISX-B experiment[19] achieves preionization densities of 3-5 x $10^{12}$ $cm^{-3}$. Runaway production, $V_1$, volt-second consumption, and impurity radiation are all reduced. A change in $dI_p/dt$ of a factor of 1.7 occurs between the ECR assisted and unassisted discharges.[20] Reference 12 predicts a reduction of startup $V_1$ by a factor of five, with 120 kW of ECR



power. This reduction requires a small radius plasma created with ECR preionization at the outboard limiter. The current and full bore ionization are obtained with a gradual rise of $V_1$ to avoid skin currents. This lowers the inductive component of the startup $V_1$. The experiments were unable to completely address this scenario.

The JIPP-T-2 stellarator-tokamak preionization experiment[18] has shown similar results. $V_1$ reduction, savings of volt-seconds, and reduction of HXR bursts were reported. ECR power of 13 kW at 35.5 GHz was injected for 15 ms.

### b. Non-microwave Techniques

Plasma guns dominate the high density techniques not using the ECR. If the gun plasma can be efficiently trapped, the directed energy of the ions will thermalize. Warm ions, at startup, might couple to early application of ICRH.

General Atomic's dc Octopole ran in a Tokapole mode with a coaxial gun as a plasma source.[21] The four, coaxially-fed internal hoops provide the toroidal electric field and divertor configuration. Parameters were R = 1.48 m, $B_t$ =430 G, $n_e$ = 3 x$10^{11}$, $I_p$ =4 kA, and $E_t$ = 0.25 V/m. A $B_v$ of a few gauss aids equilibrium. Discharge characteristics are sensitive to field

errors. Careful hoop current adjustments are required for optimum discharge parameters.

Two other examples of gun preionization have been accomplished at Nagoya University. The SPAC[22] series of devices have used rail and coaxial plasma guns to produce a target plasma for a relativistic electron beam, REB. Densities of $4 \times 10^{12} cm^{-3}$ have been produced before REB injection. The HYBTOK-I[23] experiment uses an octupole field generated by external conductors. Two co-axial guns provide a helium plasma for ohmic heating. Initial $V_1$ considerations are not discussed, but the $V_1$ at steady state was 53-88 V/m. This is high for a tokamak.

An rf technique at high density and Alfven frequencies, has been reported. The R-05 tokamak is a hybrid stellarator.[24] Using the available rf the pre-current plasma density reaches $1 \times 10^{13}$ $cm^{-3}$. The initial $V_1$ is reduced.

An alternative use of ECR was independently suggested, but could not be tested on this site. An ECR plasma could serve as a target plasma for non-inductive current drive schemes.

WT-2[25] uses an ECR preionization plasma as a target for lower hybrid current drive, LHCD. 30 kW at 35.6 GHz create a plasma of $n_e = 2 \times 10^{12}$ $cm^{-3}$ and $T_e = 5$-10 eV. 100 kW of LHCD at 915 MHz drives 5 kA of plasma current.



The Advanced Concept Torus (ACT-1), at Princeton, has used ECR preionization as a target plasma for LHCD[26]. Vertical field coils and a pre-injection density of $2 \times 10^{10}$ $cm^{-3}$ are needed. The helium pre-injection plasma is produced by ECR preionization at 9 GHz (200 W) and a hot tungsten filament.

PLT LHCD[27] experiments report 100 kA plasma currents with no target plasma previous to rf application. Presumably, the fill gas is broken down by the antenna near field or by arcing. Future plans include using an ECR plasma as a target.

## 4B. Tokapole II Startup Experiments

This section is the core of the thesis. The most successful method of assisted startup is ECR preionization. A zero-D code models the startup and compares favorably with the experiment. ICRH and plasma gun startup support the density dependence of beneficial effects suggested by the code. Some alternative methods of applying ECR assisted startup are also discussed. The experiments using the standard tokamak breakdown technique of inductive breakdown are discussed first.

### 4B1. Inductive Startup: Low Density Preionization

Tokapole II can rely on unassisted, inductive breakdown to form its discharge. The development of $n_e$, $I_p$, and $V_l$, for an unassisted startup, are shown in Figure 4.1 to illustrate the three stages of standard tokamak startup. Figure 4.1 may be compared to Figure 1.1 which is an idealized version of startup.

Vertical magnetic fields were used to examine the effect of field errors on inductive startup, as was done for the pre-current plasma confinement (3C8.a). A single coil of ten turns was wound to supply an axisymmetric field error, $B_{err}$.



Figure 4-1. Experimentally-observed stages of startup without preionization. This should be compared to the schematic representation in Fig. 1-1.

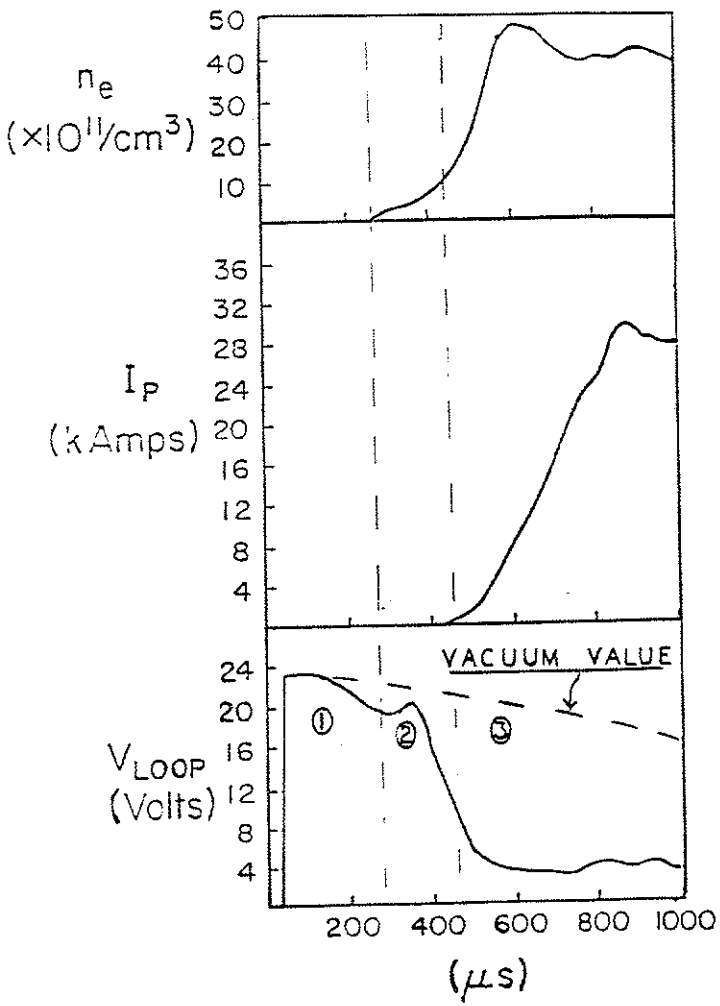




Delay to detectable plasma current, $t_d$, is the time lapse between $V_1$ application and the detection of 1.6 kA of current. $t_d$ is taken as a figure of merit of confinement for the ionizing electrons during startup. The error coil was expected to increase $t_d$ by increasing the losses along field lines.

A vacuum $V_1$ of 20 volts ($E_t$ = 6.4 V/m) is chosen for this series of experiments. The direction and magnitude of $B_{err}$ are changed, while $I_p$ is monitored. A minimum in $t_d$ occurs for $B_{err}$ = 12 G at the coil axis. Either the applied error fortuitously cancels a $B_t$ error or it compensates for the toroidal drifts during startup. An estimate of 10 G was obtained for the $B_1$ necessary to compensate drifts, on Tokapole, in section 4a1. The single coil and associated current source could not produce enough error field to demonstrate an upswing in $t_d$ after the minimum.[9] Figures 4-2 a and b present the delay time to 1.6 kA, $t_d$, as a function of the coil field at coil center. $E_t$ reversal requires $B_{err}$ reversal to maintain a minimum $t_d$. This is consistent with the reversal of the plasma current direction. Reversal of $B_t$ does not change the dependence of the delay on $B_{err}$ orientation. This indicates no axisymmetric $B_t$ error is being corrected. This agrees with the finding in 3C8.

$B_v$ coils, as described in Chapter Two, were wound to further test whether or not the $B_{err}$ was fortuitously placed to cancel a magnetic field error. A reduction of $t_d$ is obtained with the $B_v$

Figure 4-2. The time delay to a 50 mV signal on the current monitor (1.6 kA) versus the applied error magnetic field.
(a) x - standard polarities of $B_t$ clockwise (cw) and toroidal electric field, $E_t$, counter-clockwise (ccw). o - $B_t$ ccw and $E_t$ ccw.
(b) x - $B_t$ cw and $E_t$ cw. o - $B_t$ ccw and $E_t$ cw.



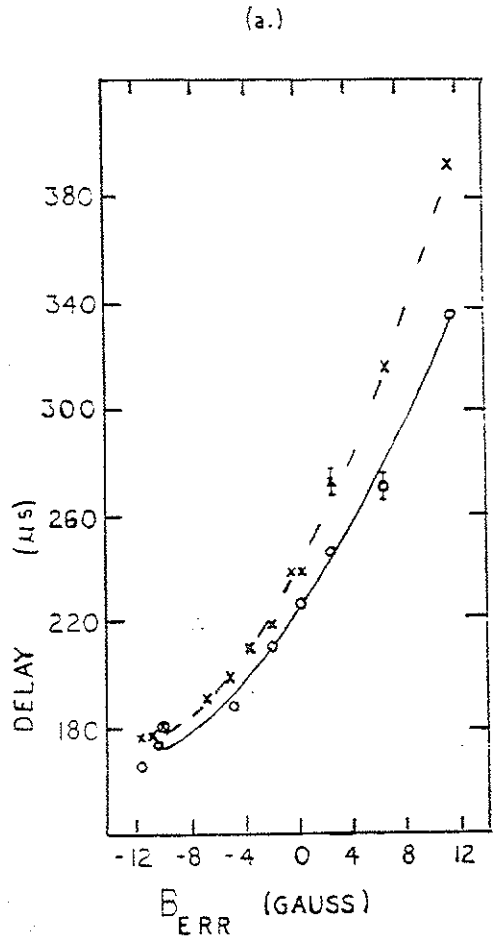

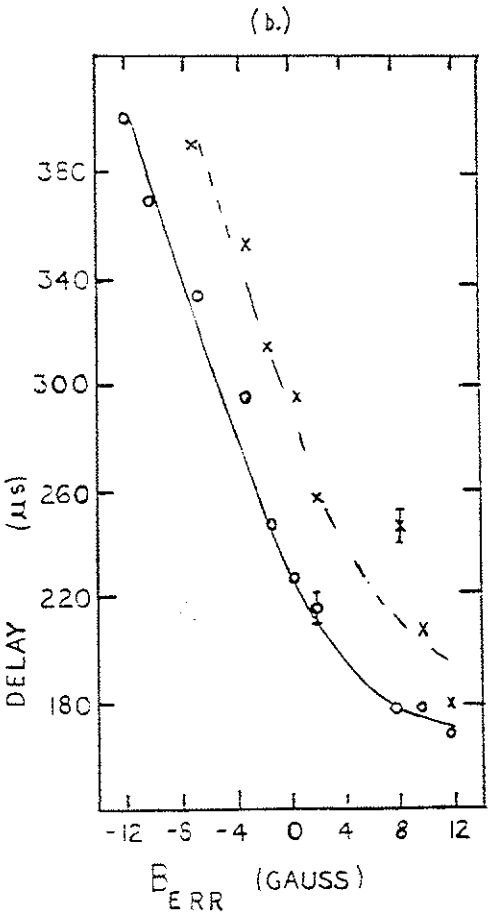




(Figure 4-3). The optimum $B_v$, with minimum $t_d$, is not a sensitive function of the applied gap voltage. Changes of $V_1$ from 16 to 20 to 24 V do not change that optimum. The change in $V_1$ does change $t_d$, because $E_t$ increases. The voltages exceed that necessary for breakdown if no losses proportional to this parameter are present. If a field error due to transformer windings or internal divertors is present, it should be proportional to $V_1$. So, such an error is not eliminated by this simple $B_v$.

If a field error is produced by $B_t$, an increase in $B_t$ will change the $B_v$ magnitude necessary for minimum $t_d$. Nearly a factor of two change in $B_t$ reduced $t_d$, but did not change the necessary $B_v$.

The insensitivity of the optimum $B_v$ to $B_t$ or $B_p$ change implies toroidal drift is the loss mechanism compensated. Thus, it is plausible that axisymmetric field errors do not limit the startup particle balance in Tokapole II.

Startup $t_d$ sensitivity to pressure is shown in figure 4.4. A variation of the optimum $B_v$ from 1 to 6 G occurs with increasing pressure. The $E_t$ is held constant. The minimum $t_d$ occurs at 4 gauss and $2.0 \times 10^{-4}$ torr.

### 4B2. Startup with ECR Preionization in Tokapole II

Figure 4-3. Reduction of time delay to detected current versus the vertical magnetic field.

| $V_1$ (vacuum value, V) | $B_r$ (kG) |
|---|---|
| 16 (x) | 3.4 |
| 20 (Δ) | 3.4 |
| 24 (o) | 3.4 |
| 20 (+) | 6.4 |



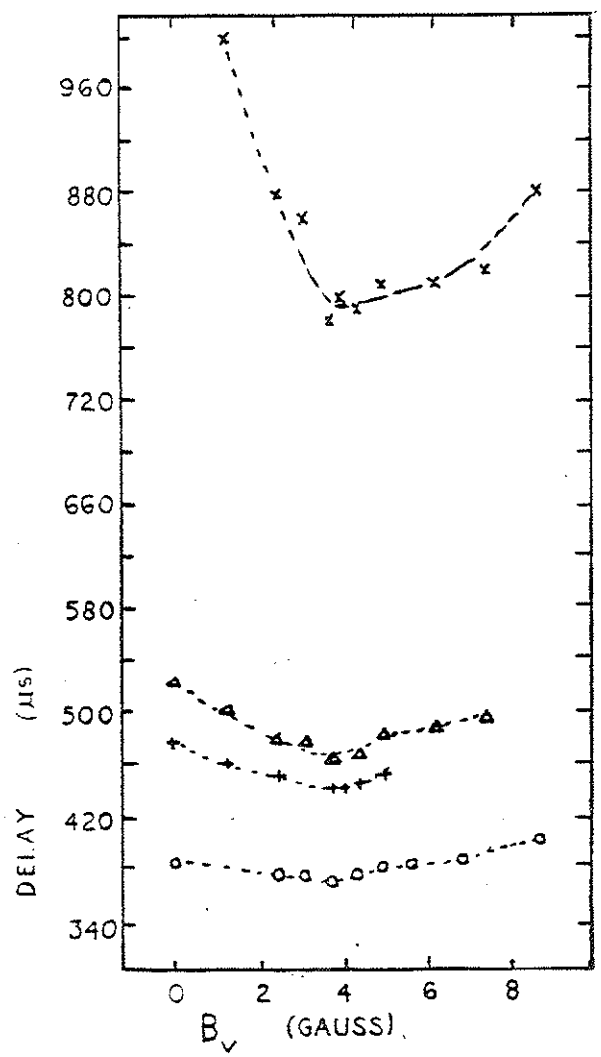

Figure 4-4. $B_v$ for minimum time delay to detected current for different fill pressures.

| Symbol | Fill Pressure |
|---|---|
| x | $0.5 \times 10^{-4}$ torr |
| o | 1.0 " " |
| Δ | 2.0 " " |
| + | 2.5 " " |
| □ | 3.0 " " |



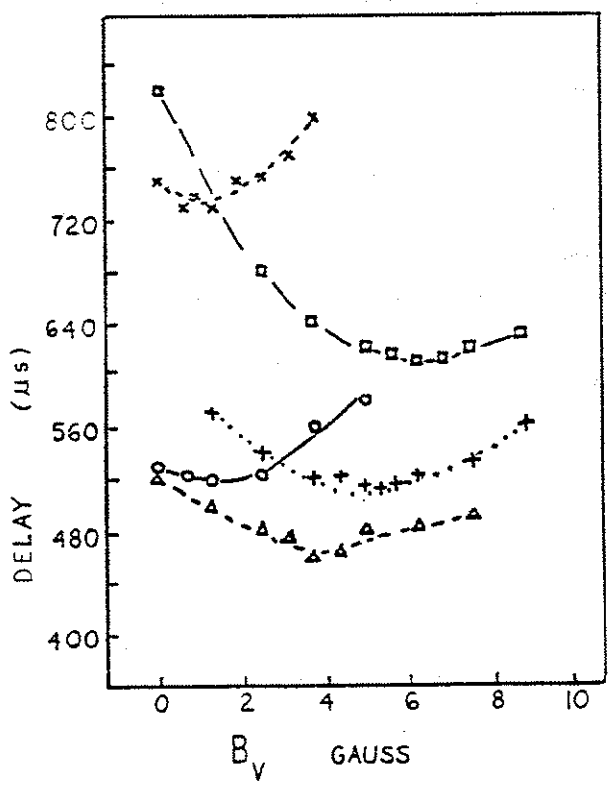

Low power ECR ( < 10 kW) preionization lowers the local $V_1$ measured by a probe by a factor of two. The quarter sine voltage waveform for startup demonstrated the reduced voltage for about 400 μs with ECR preionization (dashed curves in Figure 4-5). Current and density are detected earlier with preionization. The $V_1$ departs from the vacuum value immediately, but the initial value is reduced only 40%. This is an example of preionization density less than 1.0% of $n_o$. Comparison with Figures 1-1 and 4-1 indicate that the ECR startup produces breakdown of the gas before $V_1$ is applied. Hard x-rays detected by the midcylinder detector during current formation are eliminated with ECR preionization.

The damped $V_1$ waveform begins at a higher voltage and forms the plasma earlier. The voltage reduction is 50% with ECR preionization, and the duration is about 300 μs (Figure 4-6). In this example the microwave power is terminated, and the preionization density is allowed to decay slightly. This demonstrates the utility of the afterglow plasma for $V_1$ reduction. No difference, except for the initial density, was observed if the ECR pulse was continued after $V_1$ application.

The reduction of $V_1$ can also be demonstrated by producing similar discharges at low voltage with and at high voltage without preionization. These voltages are the vacuum voltages set by the external circuit. The internal conductors pose a



Figure 4-5. Startup $V_1$, $I_p$, and $\langle n_e \rangle$ with and without ECR preionization. The solid line represents the unpreionized startup used for Fig. 4-1. Thus, the dashed lines of the ECR preionized startup may be compared to Figures 4-1 and 1-1. Note that phase one of startup is accomplished before $V_1$ is applied. The undamped-cosine-option of $V_1$ is used in this data run.

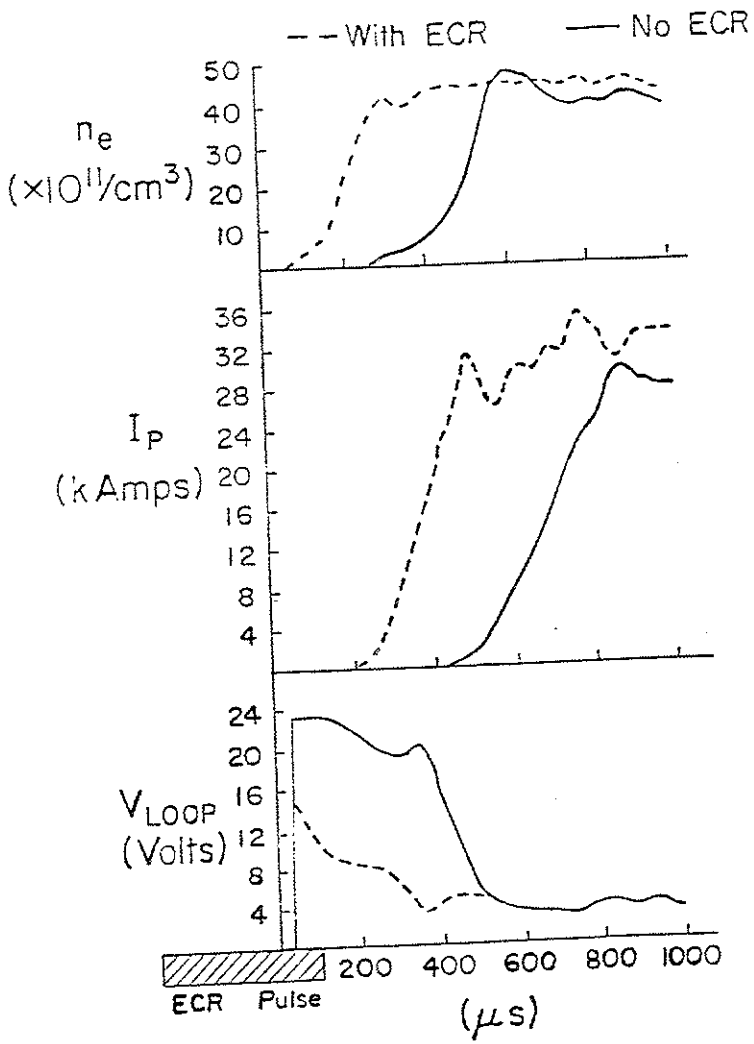




Figure 4-6. Startup $V_1$, $I_p$, and $\langle n_e \rangle$ with and without ECR preionization. The solid line represents the unpreionized startup, with the damped option for $V_1$. The plasma is clearly broken down before $V_1$ is applied.

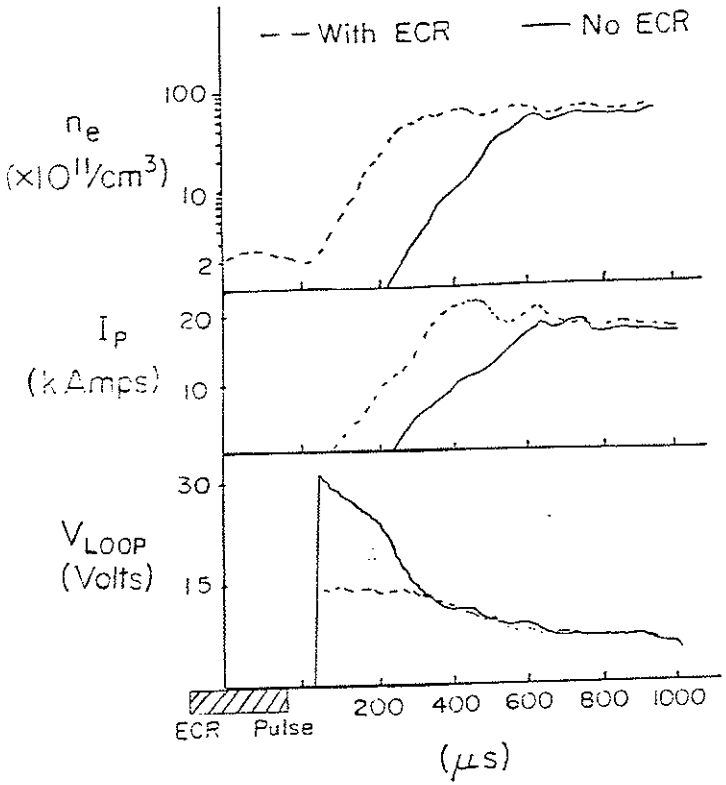




problem. The confinement and equilibrium properties are altered when their current is changed. Changing the applied gap voltage changes the internal conductor current. A typical case was 16 V (2.5 V/m) without ECRH and 10 V (1.6 V/m) with.

A spatial profile of $V_l$ reduction was made (Figure 4-7). The undamped $V_l$ waveform was used with high density preionization. Across the tokamak profile of the Tokapole, $V_l$ was reduced by about 50%. Near the wall the toroidal electric field was only slightly reduced due to the fixed externally applied voltage.

Spatial profiles of plasma current measured with a small Rogowski coil (2 cm diameter) were made. Measurements with a double-sided ion saturation current probe had more scatter but gave the same results. During the first 200 μs, with preionization, the plasma current has a very broad peak about the minor axis. At about 300 μs after the ohmic heating has been applied, the current profile becomes hollow (Figure 4-8). This is due to the high electric field near the wall. Without preionization the profile development is similar, but delayed by 200 μs.

The central current channel is fully evolved by 1.5 ms. This profile evolution is similar for startup with and without preionization. The difference is the delay to detectable current which is reduced by ECR plasma. Thus, high density preionization

Figure 4-7. Profile of the reduction of initial $V_1$, measured with a probe. This example used the undamped-cosine $V_1$ and $n_e/n_o$ ~ 2%.



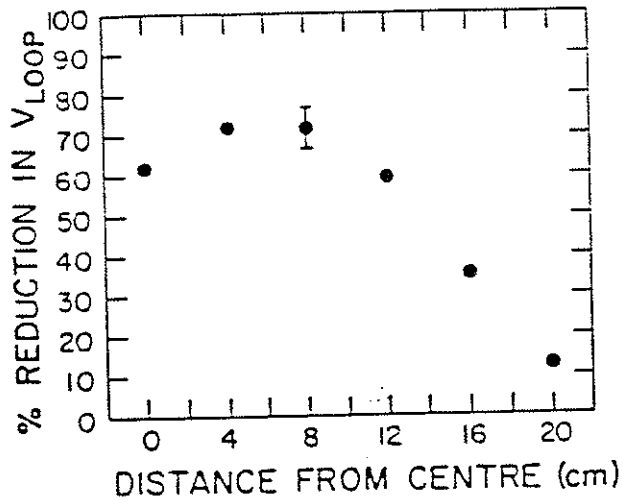

Figure 4-8. Rogowski loop profile of current during the current profile evolution from hollow to peaked-on-axis.



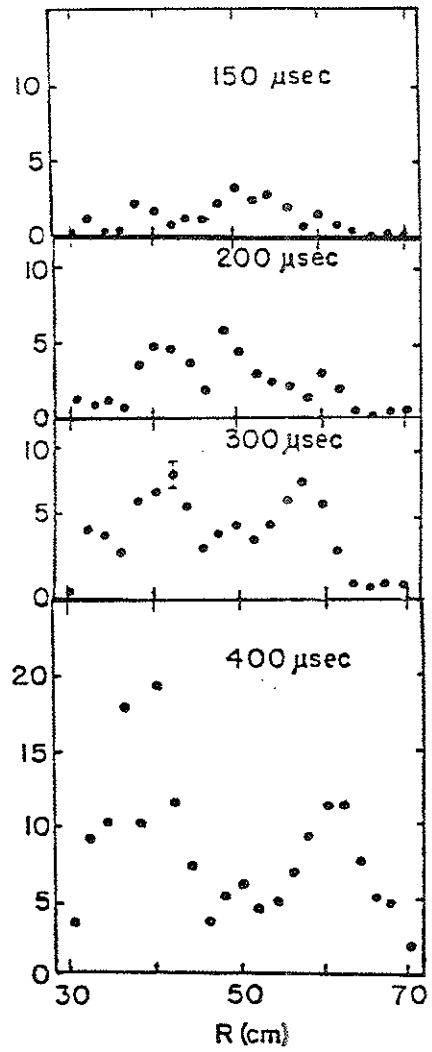

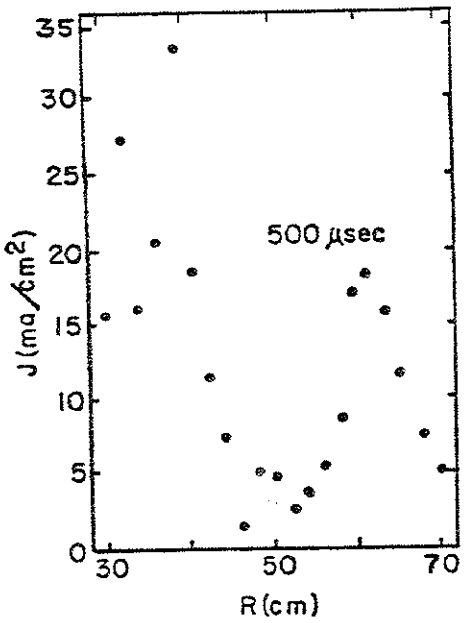




does not affect the anomalous skin effect which allows the current penetration on time scales of ~ 1 ms.

The reduction in the delay to detectable current may cause the reduction of impurity influx. Utilizing the SXR array and filtered pm-tubes, an impurity radiation profile was taken for similar discharges established by three startup scenarioes. High density ECR preionization initiates the discharge with the least delay. Application of 50 W of cw S-band microwaves also reduces the delay to detectable current. The longest delay results for inductive breakdown. The effect is a difference in the spatial evolution of impurity radiation. The least delay in current development reduces the penetration of impurities most (Figure 4-9).

Another possible explanation for impurity reduction would be a change in the floating potential and/or $T_e$ near the wall at startup. Measurements made, with N.S. Brickhouse[28] and T.H. Osborne, indicate the preionization has little effect on edge parameter magnitude, but did change the temporal development. The lack of change in magnitude is expected as a few kilowatts of preionization power should not modify the effects of the half megawatt of ohmic heating, which is supplied during startup. So, the impurity influx reduction is not due to lower edge $V_f$ or $T_e$. In fact, the edge $T_e$ may be higher with preionization. The temporal development is changed with preionization by having a

Figure 4-9. The percentage reduction of OIII radiation for low (Δ) and high (x) density preionization. During these observations, Tokapole II was not pulse-discharge cleaned, and oxygen was apparently the dominant impurity. Also, divertors (internal conductors) are a source of oxygen.



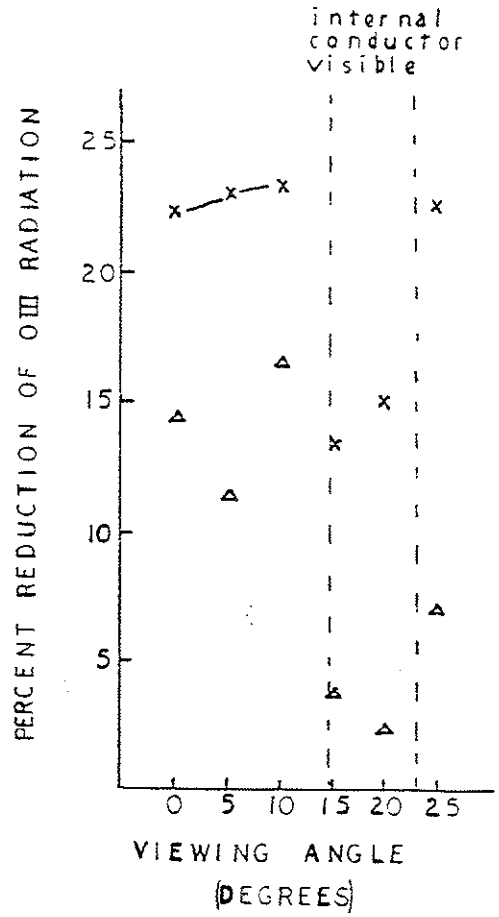

broken down plasma present when the $V_1$ is applied. The standard-startup-breakdown and plasma formation phases have very low density, poor confinement, and runaway electrons. This period has very large plasma-wall interaction rates, so the difference in impurity radiation levels with preionization lies with the earlier formation of a current channel and not a difference in edge parameters due to a change in the location of breakdown. Closing flux surfaces earlier improves confinement, which reduces the plasma-wall interaction.

The application of $B_v \geq 10^{-3} B_t$ can degrade preionization density and benefits. Without ECR preionization, $B_v$ reduces the duration of high $V_1$, but can not reproduce the immediate reduction provided by high density ECR preionization.

### 4B3. Startup Model with Preionization

The effect of $V_1$ reduction is obtained over a wide range of parameters with ECR preionization. A zero-D model is developed to explain the phenomenon, and comparisons are made to Tokapole data.

As the ECR power is only a small fraction(< 1%) of the ohmic input power, the loop voltage decrease is <u>not</u> due to replacing ohmic power for an equivalent amount of ECR power. Furthermore, the loop voltage reduction is not a sensitive function of the ECR



power level (in the range ~ 1-10 kW). ISX-B results demonstrate this to 80 kW.[19] The following set of zero dimensional equations is used to model the startup phase and reveal the cause for the loop voltage reduction:

$$V_1 = I_p R = V_v - L\frac{dI_p}{dt} \qquad (4.6)$$

$$\frac{d}{dt}\left(\frac{3}{2}n_e T_e\right) = \frac{I_p^2 R(n_e, n_o, T_e)}{Vol} - \frac{3/2 n_e T_e}{\tau_i} - P_{rad} \qquad (4.7)$$

$$\frac{dn_e}{dt} = \frac{n_e}{\tau_i} \qquad (4.8)$$

where $V_1 = I_p R$ represents the toroidal loop voltage at the plasma center, $I_p$ is the toroidal current, $V_v$ is the loop voltage that appears in the vacuum without plasma, $L \sim \mu_o R_o \left(\ln \frac{8R_o}{a} - \frac{7}{4}\right)$ is the plasma inductance, a and $R_o$ are the minor and major radii, $\tau_i = n_o \langle \sigma v \rangle$ is the ionization time, $P_{rad}$ is the radiated power density, $n_e$ and $n_o$ are the plasma and neutral density, and $T_e$ is the electron temperature. The plasma resistance $R(n_e, n_o, T_e)$

consists of a Spitzer term and a contribution from electron-neutral collisions:

$$R(n_e,n_o,T_e) = \frac{10^{-5}R_o}{a^2}\left(\frac{160}{T_e^{3/2}} + \frac{1.3n_o}{n_e}\right) \qquad (4.9)$$

where all units are MKS except $T_e$ which is in eV. Since the experimental microwave power input is small, it is neglected in eq. (4.7). Its preionizing effect appears through the initial conditions for $n_e$ and $T_e$.

The code treats the preionization plasma independent of the source. Plasma density losses are neglected since they are small relative to the ionization gain, during ohmic heating. Energy loss to the ions is neglected.

The equations evolve $n_e$, $T_e$ and I (or $V_l = I_pR$). Figure 4-10 displays the predicted loop voltage with and without preionization. The preionization density for this was 0.12% of $n_o$, which explains the initial peak. The numerical results for Tokapole II parameters exhibit $V_l$ reductions similar to that seen experimentally.

The startup plasma is neutral-dominated, as the second term is the main contributor to the plasma resistance in eq. (4.9). An increase in the startup plasma density through preionization



Figure 4-10. The $V_l$ reduction predicted by the zero-D code for a preionization density of $1.2 \times 10^{-3}\ n_o$. Comparison with Fig. 4-5 demonstrates the success of the model.

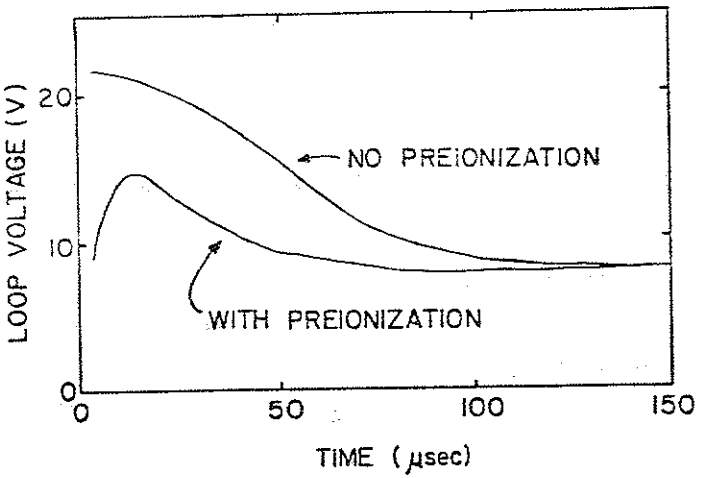




significantly raises the plasma conductivity and its time derivative, thereby reducing the loop voltage, as described below. Similar benefit is derived from preionization in reactor-sized tokamaks (Figure 4-11). Filling a volume 100 times that of Tokapole II with the required density is all that is required.

The effect is insensitive to initial temperature, as long as $n_e < 10^{-2} n_o$. An increase in $T_e$ by a factor of ten changes the Spitzer term by about a factor of 32. The neutral term is still of the same order as the lower $T_e$ Spitzer term, thus, the total change in resistance is slightly less than a factor of two.

The maximum loop voltage during startup can be obtained analytically by differentiating $V_l = I_p R$ in Eq. (4.6) with respect to time and setting the result equal to zero to give:

$$\frac{dI_p}{dt} = -I_p \frac{\rho}{R} \qquad (4.10)$$

where $\rho$ is the time derivative of the resistance, so

$$I_p R = V_v + L I_p \frac{\rho}{R} \qquad (4.11)$$

Figure 4-11. The code predicts reactor scale devices will have reduced startup $V_1$ requirements with preionization.



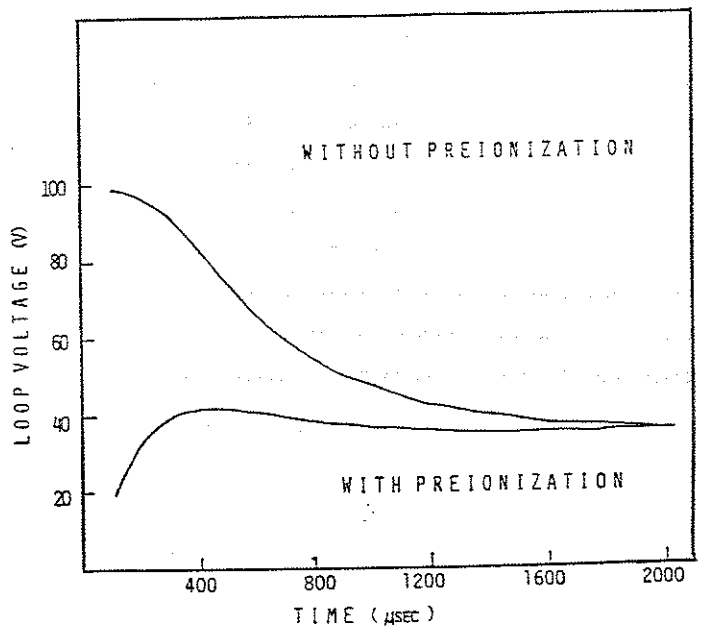

$$V_{max} = \frac{V_v}{1+(L/R)(-\rho/R)} \qquad \text{(at the extremum)} \quad (4.12)$$

This equation illustrates that it is the rate of change of the plasma resistance, ($\rho$), that produces the voltage reduction and not just the low initial resistance. When ($\rho$/R) is comparable to or greater than R/L the plasma current rises more rapidly than it would otherwise, and the plasma produces an LdI/dt term that reduces $V_l$. Since L/R is proportional to $a^2$, the result extrapolates favorably to larger devices.

For a neutral-dominated startup one can ignore eq. (4.8) and the Spitzer contribution to eq. (4.9). An analytic expression for the maximum value of the loop voltage $V_{max}$ is then easily obtained as

$$V_{max} = \frac{V_v}{1+\alpha} \quad (4.13)$$

where $\alpha = 0.1\ (\ln \frac{8R_o}{a} - \frac{7}{4}) n_e a^2 \langle\sigma v\rangle$; and all quantities are evaluated at the time when $V_l$ is a maximum. Thus for maximum $V_l$ reduction, $\alpha$ (and thus $na^2$) should be maximized during startup. This requirement ensures that the ionization time is comparable to the plasma L/R time in order that the density rise (or resistance drop) time is comparable to the rise time of $V_l$ to its



vacuum value. In fact, both the experiment and code results indicate that the peak loop voltage during a discharge decreases with increasing preionized plasma density, as shown in Figure 4-12. The effect saturates as density becomes larger because the resistivity is eventually dominated by the Spitzer term.

It is for this reason that we are able to achieve the same factor of two reduction in loop voltage at $10^{10-11}$ $cm^{-3}$ as was obtained in ISX at $>10^{12}$ $cm^{-3}$. If one considers a startup density sufficiently high that the Spitzer term dominates, then similar reduction will be allowed through a high initial conductivity and temperature, provided the temperature is not held at a constant value by radiation, so that $\rho$ is small.

### 4B4. Startup Experiment with Ion Cyclotron Frequency Assistance

An ion cyclotron resonance heating experiment in Tokapole II, provides a contrast to the ECR preionization success.[29] A few kilowatts of second harmonic ICRH power are injected into the gas. Breakdown occurs earlier, as in low density preionization, but the initial $V_l$ remains at the vacuum value. Speculation suggests ionization in the near field of the antenna is responsible and not direct coupling to the ions. The densities are too low for initial $V_l$ reduction, but volt-seconds are saved by the earlier breakdown.

Figure 4-12. The code predicts a gradual decline of required loop voltage with increasing preionization. The effect saturates at about a percent of the gas ionized. This is roughly the value at which Spitzer and neutral resistivities become of the same order for startup temperatures.

x - x-band (9 GHz) preionization

- k-band (15.5 GHz) preionization

Δ - Gun plasma preionization

o - ISX-B result[19] normalized to this curve.



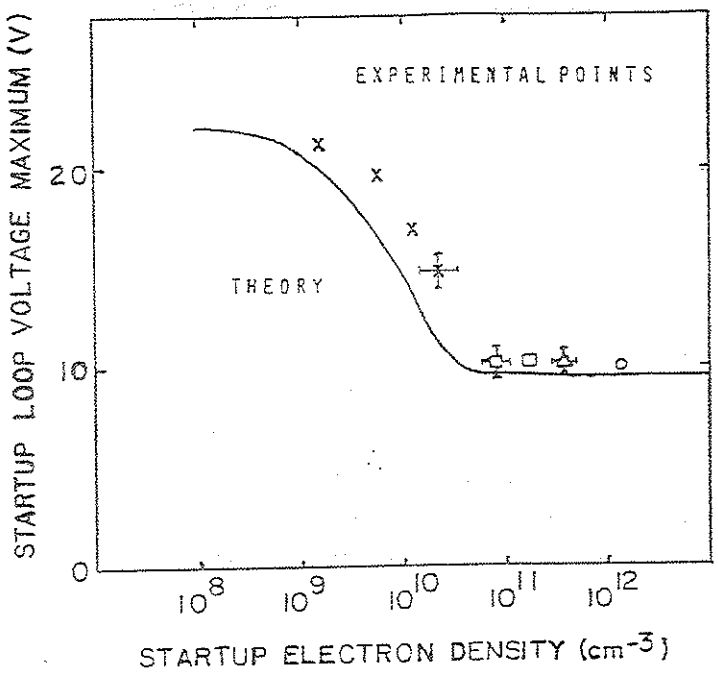

Comparison to the Pretext[10] experiments is difficult, as the $V_l$ continues to rise after the departure of the waveform from its value without plasma. This departure value is reduced by 30% from the case without the ICRH. Hot filaments as a preionization source gave a similar result to the ICRH. The reported insensitivity to ICRH power, between 0.3 and 3 kW, was attributed to increased charge-exchange for the hotter ions at higher powers.

4B5. Plasma Gun Preionization at Startup

The possibility of plasma-gun preionization was independently suggested during the course of this work. If significant gun plasma could be confined, the directed energy of the ions would be thermalized. Such a warm ion plasma might efficiently couple early ICRH power into the discharge and provide a method of burning through the the low-Z impurities. Unfortunately, at the time of these experiments the ICRH capability had been removed from Tokapole.

Early octupole field from the internal conductors aids confinement of the gun plasma. Too much octupole field (> 100 kA total divertor current) inhibits breakdown. Presumably, additional drift contributions due to $B_p$ makes breakdown more difficult. This is the same mechanism which restricts the Extrap



discharge to the narrow octupole null region.[30] The capacitor bank, which provides $V_l$, was modified to provide a power crowbar first option. The high voltage bank could then be fired. Crowbar to peak voltage exhibits a 300 μs rise time.

The optimum injection time is found to be during the rise of the high voltage waveform. Loop voltage reduction of 50% results (Figure 4-13).

In summary, loop voltage reduction with high density preionization has been demonstrated for standard tokamak operation. A zero-D model suggests ρ and initially lower resistivity are responsible. The earlier density rise and current formation phases appear to screen impurity influx and save volt-seconds. Hard x-rays are decreased by the lower loop voltage and impurity concentration. The most successful preionization method used was ECR preionization.

Figure 4-13. $V_1$ waveform with power crowbar initiated before the high voltage pulse with (dashed) and without (solid) gun preionization. This demonstrates the source independence of the loop voltage reduction by high density preionization.



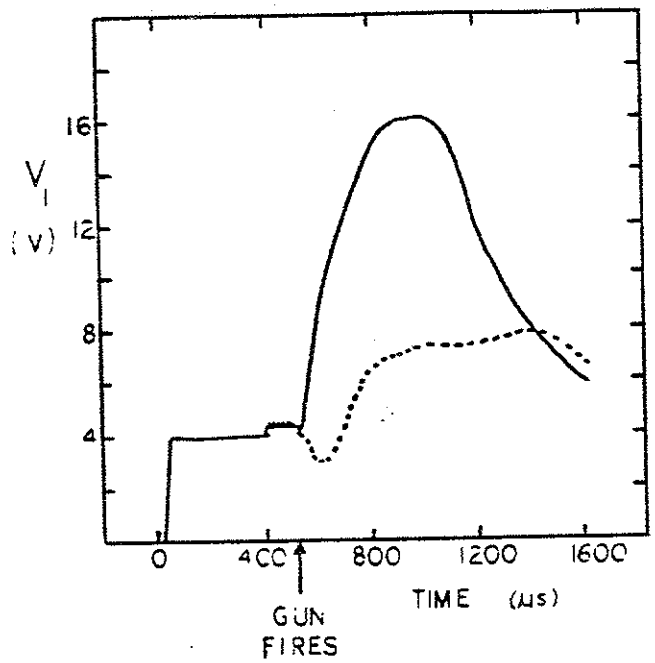

## References for Chapter Four


[1] D.J. Holly, S.C. Prager, D.A. Shepard, J.C. Sprott, Nuclear Fusion 21, 1483 (1981).

[2] L.A. Artsimovich, Controlled Thermonuclear Reactions, Gordon and Breach, Science Publishers, Inc., (1963).

[3] D.L. Dimock, H.P. Eubank, E. Hinnov, L.C. Johnson, E.B. Meservey, Nuclear Fusion 13, 271 (1973).

[4] I.H. Hutchinson, A.H. Morton, Nuclear Fusion 16, 447 (1976).

[5] J.D. Strachan, Nuclear Fusion 16, 139 (1976). 16, 345 (1976). 16, 433 (1976).

[6] A.H. Morton, J.D. Strachan, C.F. Vance, Nuclear Fusion 13 631 (1973).

[7] I.H. Hutchinson, J.D. Strachan, Nuclear Fusion 14, 649 (1974).

[8] N.V. Ivanov, I.A. Kovan, E.V. Los, Sov. Phys. Tech. Phys. 18, 326 (1973).





[9] T. Somentani, N. Fujisawa, Plasma Physics 20 1101 (1978).

[10] J.F. Benesch, University of Texas Ph. D. Thesis, (Physics), (1981).

[11] R.D. Stav, R. Callis, S. Ejima, J. Luxon, P. Petersen, T. Taylor, Bull. Am. Phys. Soc., Series II 27, 960 (1982).

[12] Y-K.M. Peng, S.K. Borowski, and T. Kammash, Nuclear Fusion 18, 1489 (1978).

[13] M. Bornatici, R. Cano, O. De Barbieri, F. Engelmann, Nuclear Fusion 23 1153 (1983).

[14] D.J. Holly, D.W. Witherspoon, University of Wisconsin Plasma Studies PLP 774 (1978).

[15] D.G. Bulyginskii, et al., Sov. J. Plasma Phys. 6 11 (1980).

[16] T. Cho, Physics Letters 77A, 318 (1980).

[17] Y. Terumichi, et al., in Proceedings of the 24th Topical Conference on RF Heating in Plasmas, University of Texas, Austin, 1981, paper D3.

[18] K. Ohkubo, et al., Nuclear Fusion 21, 1320 (1981).

[19] R.M. Gilgenbach et al., Nuclear Fusion 21, 319 (1981).

[20] A.G. Kulchar, et al., "Preionization and Start-Up in the ISX-B Tokamak Using Electron Cyclotron Heating at 28 GHz,: Oak Ridge National Lab. Rep. ORNL/TM-8713 (1983).

[21] R. Prater, et al., Phys. Rev. Lett. 34, 1432 (1975).

[22] A. Mohri, et al.: Plasma Physics and Controlled Nuclear Fusion Research 1980 (IAEA, Vienna, 1981), Vol. 1, p.511.

[23] S. Takamura, et al., Nuclear Fusion 20, 429 (1980).

[24] R.A. Demirkhanov, et al.: Plasma Physics and Controlled Nuclear Fusion Research 1982 (IAEA, Vienna, 1983), Vol. 2, p. 91.

[25] S. Kubo, et al., Phys. Rev. Lett. 50, 1994 (1983).

[26] K-L. Wong, R. Horton, M. Ono, Phys. Rev. Lett. 45, 117 (1980).



[27] F. Jobes, et al., Phys. Rev. Lett. 52, 1005 (1984).

[28] N.S. Brickhouse, Ph. D. Thesis, University of Wisconsin (1984).

[29] A.P. Biddle, Ph. D. Thesis, University of Wisconsin (1980).

[30] J.R. Drake, Plasma Phys. and Controlled Fusion, 26, 387, (1984).

Chapter Five

## Conclusions and Suggestions for Future Work

The primary results of this thesis are the demonstration and explanation of the effects of high density preionization, $n_e/n_o >$ 1.0%, on tokamak startup. The parameters reduced by high density preionization are four: startup toroidal loop voltage, $V_1$, (50%), impurity radiation (25-50%), runaway electrons (>90%), and volt-second consumption (~50%). A zero-D model simulates the density dependence of $V_1$ reduction in good agreement with experiment. The model treats the preionization plasma as an initial condition regardless of source. Favorable scaling to larger tokamaks is demonstrated by the model and the use of 9 GHz (3.2 kG) and 15.5 GHz (5.5 kG) sources.

The $V_1$ requirement is reduced by a pre-existing plasma. The resistance is lowered and the time derivative of the resistance is larger. Impurity radiation is lowered across the tokamak profile by the earlier formation of the plasma current due to preionization. Runaway electron production declines because the loop voltage is lower and fewer



electrons reach the velocity at which they decouple collisionally from the plasma. Volt-seconds used for startup are reduced by the lower $V_1$ and the shorter delay to current formation.

Three methods of preionization were tried: electron cyclotron resonance (ECR) microwaves, gun plasma injection, and ion cyclotron resonance heating (ICRH). The most successful method of high density preionization was low power (~ 10 kW) ECR microwaves. The low power produced plasma densities which achieved the benefits above. These densities did not exceed the cutoff of the ordinary mode. Thus, the microwaves were launched from the outside wall, or low field side, of the tokamak. This would be a major engineering advantage for reactor startup. High power (~ 100 kW) experiments, such as ISX-B,[1] report similar results with as much as ten times the power. The zero-D model demonstrates the saturation of $V_1$ reduction at $n_e/n_o >$ 1.0% and a bulk-ECR-plasma $T_e \sim 10$ eV. The latter seems to be common to both experiments.

The other methods used for preionization had disadvantages. The Marshall gun injects metallic impurities, and the low power ICRH only reduced the delay to breakdown and not the initial $V_1$. Marshall gun plasmas for preionization achieved $V_1$, volt-second consumption, and runaway reductions, but not impurity reduction.

This implies the benefits are dependent on the preionization density and not the source in agreement with the zero-D model. A brief experiment with ICRH for preionization, failed to obtain the benefits of high density. The discharge did form earlier, and a slight reduction in impurity radiation resulted. Presumably, the power is not as well coupled to the electrons and thus does not provide significant ionization.

The success of ECR preionization prompted power balance experiments in the toroidal magnetic field only. The measured vertical electric field ($E_v \sim 10$ V/cm) and vertical current ($I_v \sim$ 50 Amps) imply a population of warm electrons, 50 eV $\leq T_e \leq$ 1 keV. These electrons support the $E_v$ ($\sim T_e/2a$) and provide most of the vertical current. The plasma sheath at the wall prevents the vacuum vessel from shorting out the vertical electric field. However, either the fluctuations in $E_v$ or an $E_{amb} \times B$ drift in the sheath region near the wall[2] prevent a significant $E_v \times B_t$ loss. The radiation loss is inferred from measurements of hydrogen and helium plasmas. A scaling law for the ECR plasma, in a toroidal field, is favorable for larger machines ($P_\mu \sim$ scale length). This implies only a few tens of kilowatts will be necessary for reactor startup.



The Tokapole II results imply that high power preionization is no more beneficial than low power, for breakdown assistance. This depends on three criteria: field errors must be small ($\leq$ 0.1%), the warm electron population is proportional to power, and bulk plasma $T_e$ is $\sim$ 10 eV. Field errors deplete the low power plasma density, and more power might be required to compensate. The measured vertical current scales with ECR power in this experiment (up to 13 kW). The decay of the afterglow plasma indicates the bulk $T_e$ is about 5-10 eV. The triple probe measurements of $T_e \sim$ 50 eV, during the microwave pulse, are probably an indication of the warm electrons which create the $E_v$ and $I_v$. Additionally, the afterglow plasma ($T_e \sim 5$ eV) provides the same benefits for startup as the plasma with ECR power still applied. Thus, the higher power is inefficient for breakdown, but may be useful during the current-rise phase. At that time, the microwave power might replace ohmic power for impurity burn-through. More work remains to be done on the ECR plasma as a non-inductive-current-drive target. Such an experiment may provide an opportunity to study the coupling mechanisms of the current-drives to the plasma.

The Tokapole results may extend to other toroidal devices, as the JIPP-T-2 stellarator results [3] show similar benefits with ECR preionization. The proposed Wisconsin Reversed Field Pinch may also use this method. Preliminary experiments on Tokapole II in a reversed field mode are being conducted.[4] One obstacle is the comparatively low toroidal field used in reversed field pinches. Assuming the startup physics is not significantly different, the low ECR frequencies may not allow the high density regime to be achieved. The lowering of the initial $V_1$ may not be possible. But, the earlier startup allowed with low density ECR plasmas should lower the initial volt-second consumption and impurity influx. The low powers necessary for this should produce a large benefit-to-cost ratio. Additionally, once the density limit of the ECR fundamental is reached, second harmonic ECR could be tried.

The ECR plasma power balance in a purely toroidal magnetic field requires more detailed study. Measurement of the electron distribution function would be helpful. The sheath region could be studied with reference to ambipolar-electric-field-induced drift.[2] Perhaps a beam of impurity ions could be injected into



the sheath region and followed spectroscopically, if charge-exchange cross-sections are favorable. Alternatively, with the new Camac and operating system available for the Tokapole II data acquisition system, a series of fluctuation measurements could be made to determine the transport in the sheath region. Similar fluctuation measurements could also test the assumption that fluctuations, in $E_v$, prevent net transport that might be expected from the measured $E_v$.

## References for Chapter Five

[1]R.M. Gilgenbach et al., Nuclear Fusion 21, 319 (1981).

[2]S.K. Borowski, Y-K.M. Peng, T. Kammash, "RF-Assisted Start-Up in the Fusion Engineering Device (FED)," Oak Ridge National Lab. Rep. ORNL/TM-8319 (1982).

[3]K. Ohkubo, et al., Nuclear Fusion 21, 1320 (1981).

[4]J.C. Sprott, private communication.